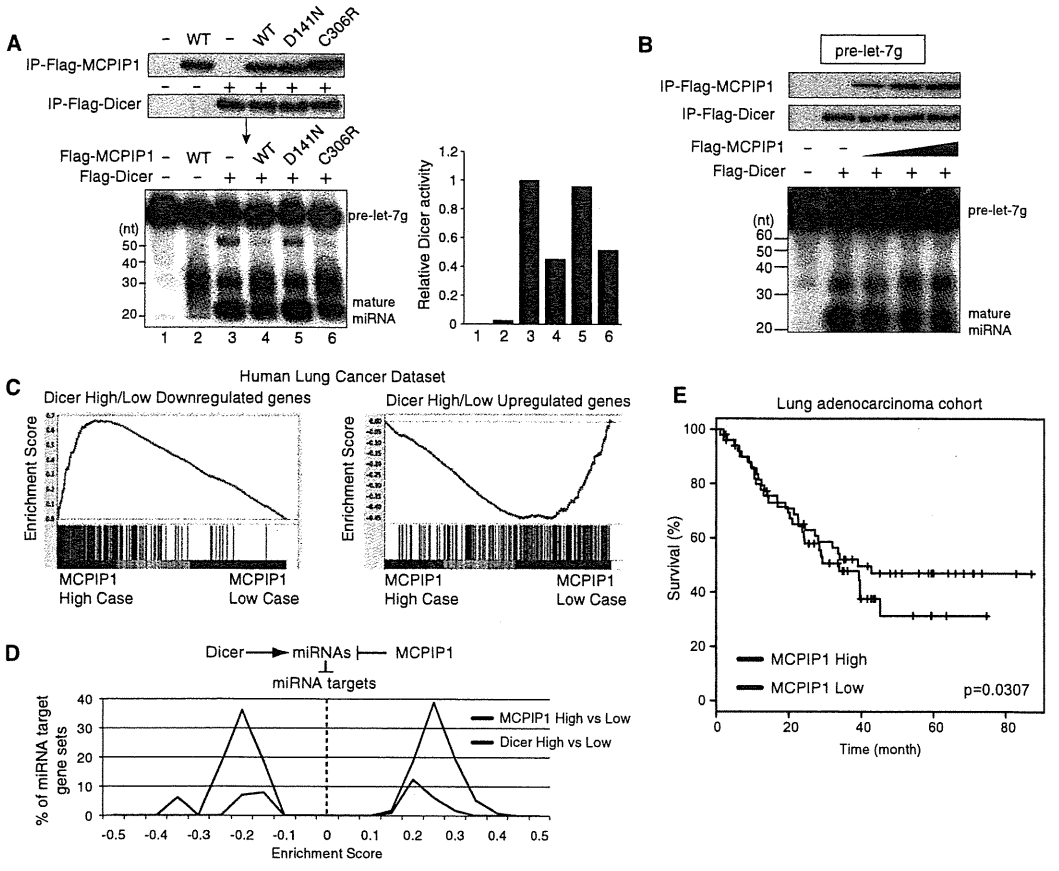

Figure 4. Antagonism between MCPIP1 Ribonuclease and Dicer and Its Implication in Human Cancer

(A and B) In vitro competition analysis using FLAG-Dicer, FLAG-MCPIP1 mutants (A), or increased amounts of FLAG-MCPIP1 (B) and radiolabeled pre-let-7g. Cleaved mature miRNAs are quantified as relative Dicer activity (A, right).

(C) Gene set enrichment analysis (GSEA) for genes negatively or positively associated with Dicer expression ("Dicer High/Low Downregulated or Upregulated genes"), along with the patients with high and low MCPIP1 expression ("MCPIP1 High Case" versus "MCPIP Low Case"), in the cohort of lung adenocarcinoma patients (Bild et al., 2006). Genes negatively or positively associated with Dicer expression were enriched in MCPIP1-High group and MCPIP1-Low group, respectively.

(D) Global histogram showing distribution of GSEA enrichment scores for the putative miRNA target gene sets in the lung adenocarcinoma cohort (Bild et al., 2006). In the comparison between Dicer-High and -Low groups, large proportion of miRNA target gene sets were underrepresented in Dicer-High group. In contrast, opposite asymmetrical distribution was observed in the comparison according to MCPIP1 expression, supporting the antagonism between Dicer and MCPIP1.

(E) Kaplan-Meier plots representing the survival probability in the same dataset, according to low or high MCPIP1 expression levels. The log-rank test p value reflects the significance of the association between high MCPIP1 expression and poor prognosis. See also Figure S4.

cleavage by MCPIP1 in vitro (Figure 6D), strengthening the importance of terminal loop as a target of MCPIP1.

While MCPIP1 has recently been shown to promote the mRNA decay of IL-6 (Matsushita et al., 2009), we noticed that the target element of IL-6 3′ UTR forms a stem-loop structure similar to pre-miRNAs (Matsushita et al., 2009; Paschoud et al., 2006) (Figure 6C, right). We similarly cloned the IL-6 3′ UTR fragments cleaved by MCPIP1 in vitro, and found that the ends of recovered 5′ and 3′ fragments were distributed in 5′- and 3′-franking regions of the hairpin structure, respectively (Figure S6D), supporting the idea that MCPIP1 preferentially targets the hairpin structure. We then investigated structural features of MCPIP1 target RNAs by generating a range of pre-miRNA mutants with various lengths of stem and terminal loop. As a result, deletion analysis showed that MCPIP1 could cleave pre-miRNA mutants with various stem lengths (Figures 6E and S6E), while deletion of the loop region affected MCPIP1 action in vitro, and MCPIP1 could not cleave pre-miRNA mutants without a loop region (Figures 6F and S6F, see d5–7 mutants). These findings thus suggest that MCPIP1 potentially controls the destinies of various hairpin RNAs. This notion parallels the finding that the Drosha-DGCR8 complex cleaves the hairpin structure in DGCR8 mRNA, as well as pri-miRNAs (Han et al., 2009). These observations imply the presence of dynamic crosstalk between the pathways for mRNA stability control and miRNA biogenesis.

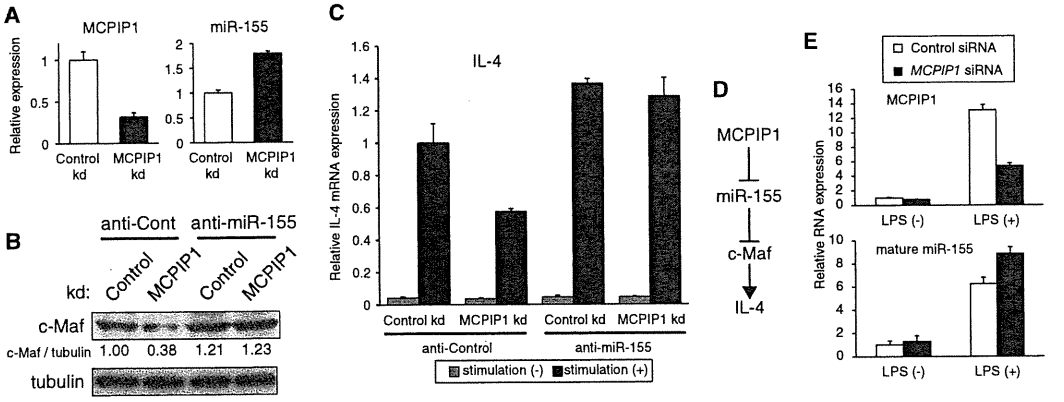

Figure 5. Modulation of miR-155/c-Maf Axis by MCPIP1

(A) miR-155 upregulation by MCPIP1 knockdown in Jurkat cells. Jurkat cells were transduced with MCPIP1 knockdown lentivirus vector (MCPIP1 kd) and analyzed by qRT-PCR analysis.

(B) miR-155-dependent c-Maf suppression by MCPIP1 depletion, as assessed by immunoblot analysis of c-Maf under a combination of MCPIP1 knockdown and transfection of anti-miR-155 inhibitor in Jurkat cells.

(C) Effects of MCPIP1 and miR-155 suppression on IL-4 induction by stimulation with PMA and ionomycin. Jurkat cells were prepared in the same combination as in (B) and analyzed by qRT-PCR analysis.

(D) Relationship of MCPIP1/miR-155/c-Maf/IL-4 axis.

(E) Involvement of MCPIP1 in LPS-mediated miR-155 upregulation in THP-1 macrophage cells, as assessed by qRT-PCR analysis after transfection with control siRNA or *MCPIP1* siRNA. See also Figure S5. Error bars represent SEM.

Oligomerization of MCPIP1 Ribonuclease via the Vertebrate-Specific C Terminus

In our study, other MCPIP family proteins (MCPIP2, MCPIP3, and MCPIP4) showed little effect on miRNA activity in spite of the presence of the conserved NYN domain and CCCH motif (Figures 1A, 7A, and S7A). Together with the differential effects of C306R mutation on in vitro and in vivo activities of MCPIP1 (Figures 3D–3G), these observations raised the possibility that other domain(s) including CCCH motif, besides the NYN domain, could be important for the in vivo function of MCPIP1. Besides the NYN domain, the CCCH zinc-finger domain and proline rich domain are placed at the central region and C-terminal region of MCPIP1, respectively (Figure 7A). In *C. elegans* and *Drosophila*, a similar protein with MCPIP1, C30F12.1 and CG10889, respectively, is observed (Figure 7A). These molecules lack a proline-rich domain found in MCPIP1 C terminus, and the C terminus of vertebrate MCPIP2/3/4 also shows little similarity with the MCPIP1 C terminus, suggesting that the C terminus of MCPIP1 has emerged as a certain functional domain in the vertebrate MCPIP gene family (Figure 7A).

Previous studies have demonstrated that some RNases and RNase domains, including RNase A and RNase L, function in the oligomerized state (Bergdoll et al., 1997; Salehzada et al., 1993). RNase A has been shown to oligomerize via a proline-dependent arm exchange mechanism (Bergdoll et al., 1997). Dicer has also been shown to function through intramolecular dimerization of its two RNase III domains (Zhang et al., 2004).

On the basis of these findings, we examined the possibility of MCPIP1 oligomerization via the unconserved C-terminal region including the proline-rich domain. While human MCPIP1 was usually observed as a 66 kDa monomer, the protein was detected as a high molecular weight complex of about 200 kDa under chemical crosslinking by disuccinimidyl suberate (DSS) (Figure 7B). Blue native PAGE analysis revealed that overexpressed and endogenous MCPIP1 proteins mainly exist as complexes of about 200 kDa, and of about 220 kDa and 600–700 kDa, respectively (Figure 7C). Immunoprecipitation analysis also detected an additional band of FLAG-tagged MCPIP1 with about 400 kDa in blue native PAGE (Figure 7D). Since these FLAG-MCPIP1 complexes were coimmunoprecipitated with cointroduced HA-tagged MCPIP1 (Figures 7B and 7D), these complexes may represent oligomeric forms of MCPIP1. In addition, endogenous MCPIP1 complexes of about 220 kDa and 600–700 kDa showed higher molecular weights than two FLAG-tagged MCPIP1 complexes of 200 kDa and 400 kDa, suggesting the presence of additional partner protein(s) interacting with endogenous MCPIP1. The conventional immunoprecipitation experiments confirmed the association between FLAG-tagged and HA-tagged MCPIP1 molecules (Figure S7B) and revealed that this oligomerization required the C-terminal region (Figures S7C and S7E). In accordance with the results, these C-terminal deletion mutants also showed reduced miRNA suppressor activities (Figures 7F, 7G, S7D, and S7E). Furthermore, RNA immunoprecipitation analysis clarified that both the CCCH motif and vertebrate-specific C terminus are important for efficient interaction between MCPIP1 and pre-miRNA in vivo, although the NYN domain has a minor role in this aspect (Figure 7H). We further observed that D141N and C306R mutants showed little dominant-negative effects on the function of wild-type MCPIP1 both in vivo and in vitro (Figure S7F). Collectively, MCPIP1 harbors several functional domains to inhibit miRNA maturation efficiently (Figure 7I). The presence of the vertebrate-specific MCPIP1 C terminus suggests that the

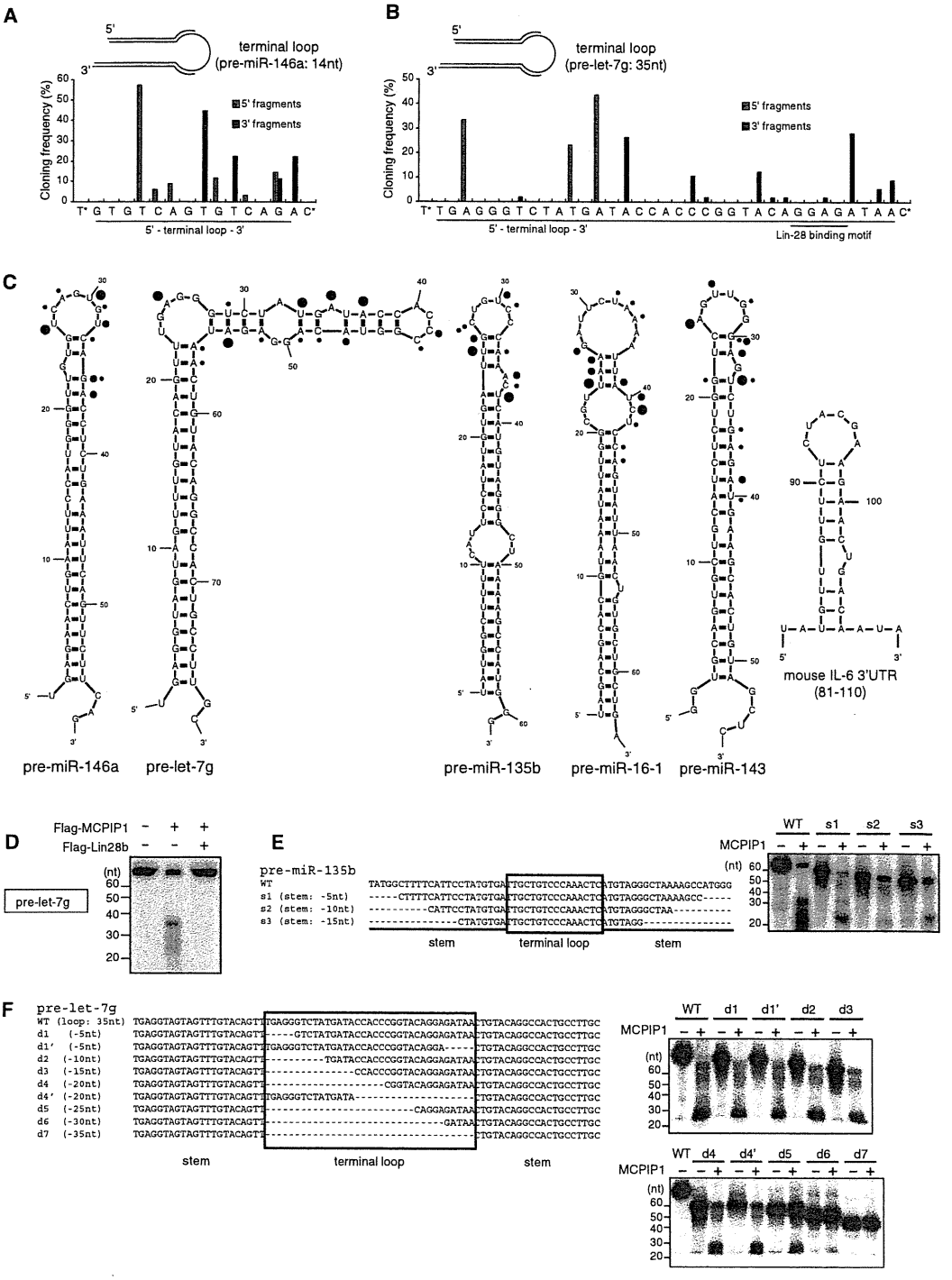

Figure 6. Targeting of the Terminal Loops of Pre-miRNAs by MCPIP1 Ribonuclease

(A and B) Cloning analysis of MCPIP1-cleaved pre-miRNA fragments. After in vitro cleavage reaction (90 min), the cleaved fragments of pre-miR-146a (A) and pre-let-7g (B) were cloned and sequenced. 5′ and 3′ fragments indicate the fragments composed of 5′ and 3′ mature miRNA strand and additional bases within the terminal loop, respectively. The data about pre-miR-135b, pre-miR-143, and pre-miR-16-1 are shown in Figures S6A–S6C.

(C) Comparison of the sequence analyses of MCPIP1-cleaved fragments (A and B and Figures S6A–S6C) and secondary structure prediction (Zuker, 2003). The ends of 5′ and 3′ fragments are indicated by blue and red circles, respectively. The structure of MCPIP1 target sequence of mouse *Il6* 3′ UTR (80–110) is also shown.

MCPIP family has evolved an anti-miRNA function of MCPIP1 in vertebrates.

DISCUSSION

Here we identified the CCCH zinc-finger ribonuclease MCPIP1 as an important RNase, which counteracts the productive miRNA biogenesis directed by two RNases, Drosha and Dicer (Figure 7J). It is poorly understood how the half-lives and absolute levels of mature miRNAs are determined, in comparison with advances concerning the mechanisms of miRNA production. Recent reports revealed that several nucleases, such as SDN in *Arabidopsis* and XRN-2 in *C. elegans*, degrade mature miRNAs (Chatterjee and Grosshans, 2009; Ramachandran and Chen, 2008). The present study first demonstrated that not only mature miRNAs but also pre-miRNAs are targets of active degradation to reduce miRNA activities. Considering that MCPIP1 expression dynamically changes during the inflammatory response (Liang et al., 2008a; Liang et al., 2008b), the rate of de novo miRNA synthesis might be actively regulated through the pre-miRNA decay by MCPIP1. Accordingly, global downregulation of miRNAs including miR-16 (as also demonstrated in Figure S5C) and overall shortening of mRNA 3′ UTRs have been observed along T cell activation (Sandberg et al., 2008; Wu et al., 2007).

Open questions remain regarding how MCPIP1 recognizes pre-miRNAs and preferentially inhibits the miRNA pathway and whether MCPIP1 uniformly acts on individual miRNAs. While further investigation is important, our trial analysis of RNA-IP/sequencing experiments suggested that the MCPIP1 D141N mutant interacts with a range of miRNA precursors and transcripts including IL6 (Figures S7G and S7H). On the other hand, the expression levels of externally expressed DGCR8 mRNA and IL-6 3′ UTR RNA both containing a hairpin structure decreased to about 50% by MCPIP1 overexpression (Figure S7I, left), as well as pre-miRNAs, but MCPIP1 knockdown only slightly upregulated the endogenous DGCR8 and IL-6 mRNA levels and also failed to show significant or consistent effects on other RNA species such as Alu and tRNAs (Figure S7I, right), in contrast to the effects on endogenous mature miRNAs. Considering that MCPIP1 decreased overexpressed pre-miRNAs by about half and their mature forms by about one-tenth (Figure 1), these results suggest that the miRNA biogenesis pathway is more susceptible to MCPIP1 regulation than other RNA species, maybe because of the requirement for stepwise collaboration of multiple maturation processes. Differential localization of MCPIP1 and various RNA species may also contribute to the strong inhibitory impact of MCPIP1 on the miRNA pathway. In addition, heterogenous effects of MCPIP1 knockdown on individual mature miRNAs (Figures 2G and 2H) might be attributable to intrinsic properties of MCPIP1, as influenced by preferential target structures/sequences and additional partner protein(s), or complexity of regulation of each miRNA modified by various factors, including pri-miRNA transcription, Drosha processing, cytoplasmic export, Dicer processing, existence of specific RNA-binding proteins, and miRNA stability regulation.

Lin-28 interacts with the terminal loop of let-7 precursor and specifically hinders let-7 maturation. In addition, several other RNA-binding proteins such as hnRNP A1 and KSRP also interact with the terminal loops of miRNA precursors and rather facilitate the processing of pri-miRNAs and/or pre-miRNAs. Considering that MCPIP1 targets the terminal loop of pre-miRNAs, these RNA-binding proteins might protect miRNA precursors from the degradation in addition to their intrinsic function in miRNA biosynthesis. Since the loop region is largely considered dispensable for the basic action of Drosha and Dicer, the evolutionarily conserved loops of many miRNA precursors might contain regulatory information for active degradation to differentially generate distinct miRNA species.

Our results demonstrated the importance of the C terminus for MCPIP1 function and its poor conservation between invertebrates and vertebrates (Figure 7). These findings suggest that the vertebrate MCPIP family has diversified and evolved an anti-miRNA function of MCPIP1. Although miRNA and RNAi pathways and their components are well conserved across a wide range of species, previous studies suggested certain evolutional differences, in particular from immunological aspects, as represented by different major antiviral mechanisms between plants/invertebrates and mammals, i.e., respectively, RNAi response and interferon (IFN) response (Umbach and Cullen, 2009). In addition, miRNAs encoded in certain mammalian viruses perturb host gene regulatory networks and there exist several mechanisms represented by RNase L and ZAP to avoid the promiscuity by viral-derived RNA species in vertebrate cells (Sadler and Williams, 2008). The presence of MCPIP1-mediated abortive processing machinery and diversity of MCPIP1-related genes, taken together with these findings, may therefore imply dynamic evolutional transition of RNA silencing system.

In the present study, we have intriguingly found an inverse correlation between MCPIP1 and Dicer function in human lung cancer cohorts (Figures 4C–4E and S4). Importantly, we observed an association of high MCPIP1 expression with poor survival, suggesting the usefulness of MCPIP1 as a prognostic marker. MCPIP1 upregulation by several inflammatory stimuli, including MCP1, might be partly attributable to global miRNA downregulation in cancer, in addition to reduced expression of Dicer and/or Drosha and mutations in TRBP and XPO5. Future studies may provide useful information about involvement of MCPIP1 in miRNA dysregulation in human malignancies and important insights for the efficiency of RNA-based therapeutics. In conclusion, the present work provides a clue for the comprehensive understanding of miRNA dynamics during the

(D) Effect of Lin-28b addition on MCPIP1 activity targeting pre-let-7g.
(E) Effect of the stem length of pre-miRNA on MCPIP1 activity. (Left) The sequences of deletion mutants of pre-miR-135b with various lengths of stem region. (Right) In vitro cleavage assay by coincubation of radiolabeled pre-miR-135b mutants and FLAG-MCPIP1 for 90 min.
(F) Effect of the terminal-loop length of pre-miRNA on MCPIP1 activity. (Left) The sequences of deletion mutants of pre-let-7g carrying a long terminal loop (35 nt). (Right) In vitro cleavage assay by coincubation of radiolabeled pre-let-7g mutants and FLAG-MCPIP1 for 120 min. See also Figure S6.

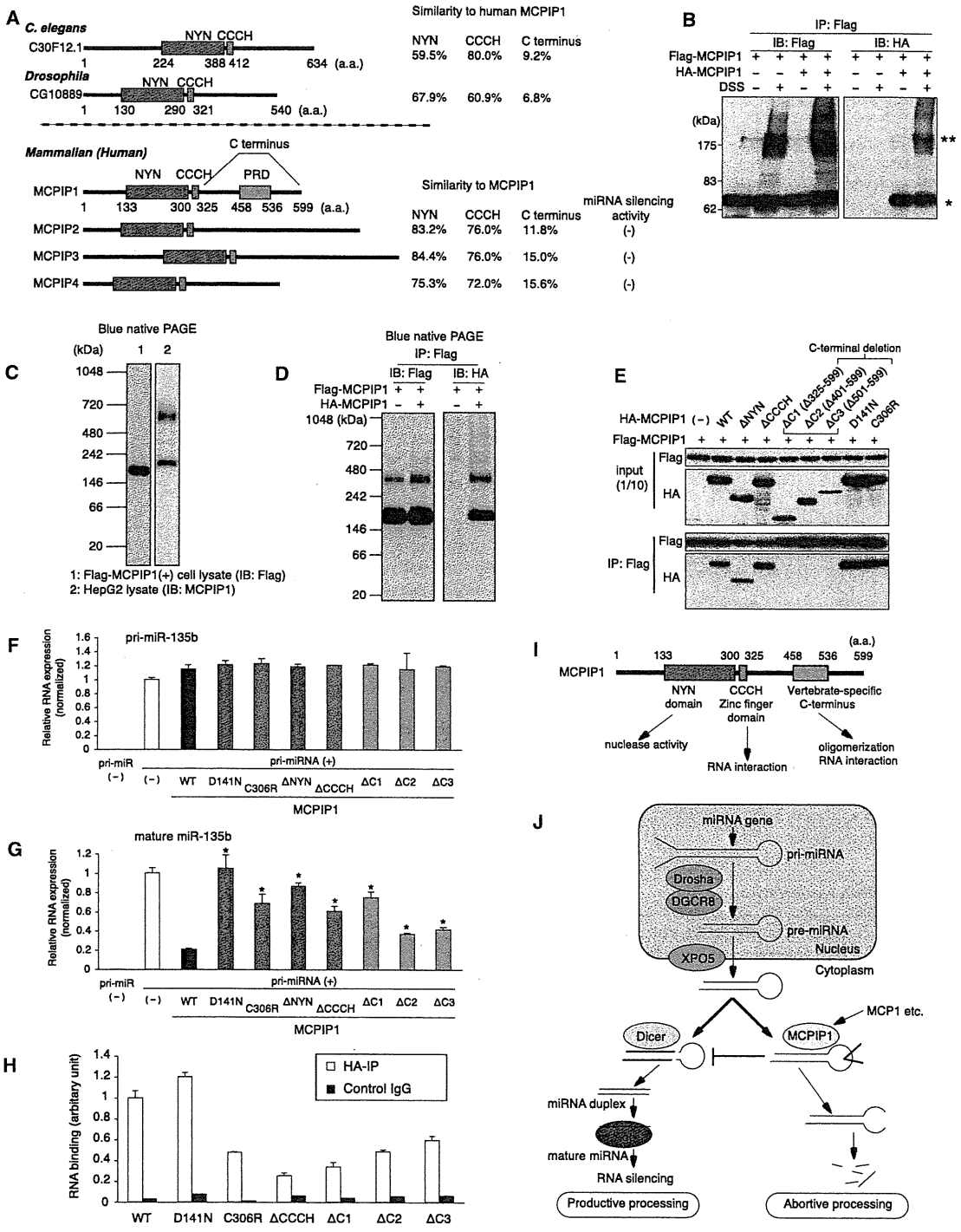

Figure 7. Oligomerization via Vertebrate-Specific C Terminus Is Important for miRNA Silencing Activity of MCPIP1

(A) Schematic representation of human MCPIP family proteins and invertebrate MCPIP1-related proteins (*C. elegans* C30F12.1 and *Drosophila* CG10889). The numbers on the right indicate the sequence similarity to human MCPIP1 protein.

(B) Oligomerization of MCPIP1. FLAG-MCPIP1 and HA-MCPIP1 were ectopically expressed in HEK293T cells. Cell lysates were crosslinked with DSS and immunoprecipitated with the anti-FLAG antibody followed by immunoblotting. Asterisks (*, **) indicate MCPIP1 monomers and oligomers, respectively.

physiological and pathological processes, such as inflammation and cancer.

EXPERIMENTAL PROCEDURES

Cell Lines, Antibodies, and Reagents

HEK293T, HepG2, Jurkat, and THP-1 cell lines were obtained from the American Type Culture Collection. HEK293T and HepG2 cells were maintained in Dulbecco's modified Eagle's medium (GIBCO) containing 10% fetal bovine serum (FBS). Hematological cell lines were maintained in RPMI1640 medium (GIBCO) with 10% FBS. Plasmids, antibodies, and reagents are described in the Supplemental Experimental Procedures.

Luciferase Reporter Assay, qRT-PCR Assays, and Northern Blot Analyses

Dual renilla/luciferase assays, qRT-PCR assays, and northern blot analyses were carried out as previously described (Suzuki et al., 2009). The expression levels of mature miRNAs were determined using TaqMan MicroRNA assay kit (Applied Biosystems) according to the manufacturer's protocol. The primer sequences used and related procedures are described in the Supplemental Experimental Procedures.

Immunocytochemistry

Immunostaining was carried out with anti-HA antibody, followed by counterstaining with TOTO-3 (Invitrogen–Molecular Probes). Stained specimens were examined using a LSM 510 META confocal microscope (Carl Zeiss).

In Vitro Pre-miRNA Cleavage Assay

In vitro pre-miRNA cleavage assay was performed modifying the method of in vitro pri-miRNA processing assay described previously (Suzuki et al., 2009). α^{32}P-UTP-internally-labeled pre-miRNAs were generated by in vitro transcription using PCR fragments containing pre-miRNA sequences fused to a T7 RNA polymerase promoter as templates. The detailed procedures are described in the Supplemental Experimental Procedures.

Immunoprecipitation and Immunoblot assay

Cells were lysed with Nonidet P-40 lysis buffer and subjected to immunoblot assay with standard procedures.

Cloning of Pre-miRNA Fragments

MCPIP1-cleaved RNA fragments were cloned and sequenced using microRNA cloning kit (Wako) according to the manufacturer's instructions. Briefly, the fragments were isolated using Trizol (Invitrogen), after in vitro cleavage reaction (90 min) without radioisotope as described above. We ligated 3′ adaptors into the RNA fragments with thermostable ssDNA ligase (Wako). The ligated substrate was reverse-transcribed, ligated with 5′ adaptors, and further PCR-amplified using HOT Goldstar DNA Polymerase (Wako). The PCR products were cloned into pCR2.1-TOPO vectors (Invitrogen) and sequenced.

RNA Immunoprecipitation Assay

RNA immunoprecipitation assay was performed as previously described (Suzuki et al., 2009).

Gene Expression Profiling Analysis

Gene expression profiling data of lung cancer patients were previously described (in Bild et al., 2006 [Figures 4C–4E], Shedden et al., 2008 [Figures S4B and S4D], and Larsen et al., 2007 [Figures S4C and S4E]), and were obtained from caArray system or NCBI's Gene Expression Omnibus. The expression levels of Dicer or MCPIP1 were evaluated by the corresponding probes. GSEA was performed with GSEA software available from the Broad Institute (http://www.broadinstitute.org/gsea/) (Subramanian et al., 2005). GSEA-embedded potential miRNA target gene sets were used. Survival analysis was performed using the survival package of R, the survfit function and the survdiff function.

SUPPLEMENTAL INFORMATION

Supplemental Information includes seven figures and Supplemental Experimental Procedures and can be found with this article online at doi:10.1016/j.molcel.2011.09.012.

ACKNOWLEDGMENTS

We thank K. Isogaya, K. Horiguchi, D. Koinuma, and T. Watabe for discussion; M. Tanaka and T. Funakoshi (Wako) for technical advice; T. Yokochi for encouragement; and all members of the Department of Molecular Pathology, at the University of Tokyo. This work was supported by KAKENHI (Grant-in-Aid for Scientific Research for Research Activity start-up [No. 22890038] and on Innovative Areas "RNA regulation" [No. 23112702]), the Global Center of Excellence Program for "Integrative Life Science Based on the Study of Biosignaling Mechanisms" from the Ministry of Education, Culture, Sports, Science, and Technology of Japan, and the Cell Science Research Foundation.

Received: March 4, 2011
Revised: June 17, 2011
Accepted: September 7, 2011
Published: November 3, 2011

REFERENCES

Anantharaman, V., and Aravind, L. (2006). The NYN domains: novel predicted RNAses with a PIN domain-like fold. RNA Biol. *3*, 18–27.

Bergdoll, M., Remy, M.H., Cagnon, C., Masson, J.M., and Dumas, P. (1997). Proline-dependent oligomerization with arm exchange. Structure *5*, 391–401.

Bild, A.H., Yao, G., Chang, J.T., Wang, Q., Potti, A., Chasse, D., Joshi, M.B., Harpole, D., Lancaster, J.M., Berchuck, A., et al. (2006). Oncogenic pathway signatures in human cancers as a guide to targeted therapies. Nature *439*, 353–357.

Chatterjee, S., and Grosshans, H. (2009). Active turnover modulates mature microRNA activity in Caenorhabditis elegans. Nature *461*, 546–549.

(C and D) Blue native PAGE analyses. HEK293T cells expressing FLAG-MCPIP1 or HepG2 cells were subjected to blue native PAGE analysis using FLAG antibody or MCPIP1 antibody (C). FLAG immunoprecipitates from cell lysates containing FLAG-MCPIP1 and HA-MCPIP1 were also analyzed by blue native PAGE analysis after elution with FLAG peptide (D).

(E) Requirement of the C terminus for MCPIP1 oligomerization. FLAG-MCPIP1 and HA-MCPIP1 mutants were ectopically expressed in HEK293T cells. Cell lysates were immunoprecipitated with the anti-FLAG antibody followed by immunoblotting.

(F and G) Effects of MCPIP1 mutation on miRNA maturation. MCPIP1 mutants were coexpressed with pri-miR-135b in HEK293T cells. At 48 hr posttransfection, the expression levels of pri-miRNA (F) and mature miRNA (G) were analyzed with qRT-PCR analyses (*$p < 0.05$, compared to wild-type MCPIP1 [WT]; n = 3).

(H) pre-miRNA binding capacity of MCPIP1 mutants. HEK293T cells were cotransfected with pri-miR-135b expression vector and various MCPIP1 mutant expression vectors. After transfection, MCPIP1 mutants were immunoprecipitated with anti-HA antibody and subjected to RT-PCR analysis with pre-miR-135b primers. As controls, RNA samples immunoprecipitated with nonspecific IgG (Control IgG; n = 3) were subjected to PCR.

(I) Differential contribution of MCPIP1 domains for miRNA silencing activity.

(J) A schematic model for the inhibition of miRNA processing by MCPIP1. See also Figure S7. Error bars represent SEM.

Costinean, S., Sandhu, S.K., Pedersen, I.M., Tili, E., Trotta, R., Perrotti, D., Ciarlariello, D., Neviani, P., Harb, J., Kauffman, L.R., et al. (2009). Src homology 2 domain-containing inositol-5-phosphatase and CCAAT enhancer-binding protein beta are targeted by miR-155 in B cells of Emicro-MiR-155 transgenic mice. Blood *114*, 1374–1382.

Davis, B.N., and Hata, A. (2009). Regulation of MicroRNA Biogenesis: A miRiad of mechanisms. Cell Commun. Signal. *7*, 18.

Han, J., Pedersen, J.S., Kwon, S.C., Belair, C.D., Kim, Y.K., Yeom, K.H., Yang, W.Y., Haussler, D., Blelloch, R., and Kim, V.N. (2009). Posttranscriptional crossregulation between Drosha and DGCR8. Cell *136*, 75–84.

Heo, I., Joo, C., Cho, J., Ha, M., Han, J., and Kim, V.N. (2008). Lin28 mediates the terminal uridylation of let-7 precursor MicroRNA. Mol. Cell *32*, 276–284.

Karube, Y., Tanaka, H., Osada, H., Tomida, S., Tatematsu, Y., Yanagisawa, K., Yatabe, Y., Takamizawa, J., Miyoshi, S., Mitsudomi, T., and Takahashi, T. (2005). Reduced expression of Dicer associated with poor prognosis in lung cancer patients. Cancer Sci. *96*, 111–115.

Kumar, M.S., Lu, J., Mercer, K.L., Golub, T.R., and Jacks, T. (2007). Impaired microRNA processing enhances cellular transformation and tumorigenesis. Nat. Genet. *39*, 673–677.

Larsen, J.E., Pavey, S.J., Passmore, L.H., Bowman, R., Clarke, B.E., Hayward, N.K., and Fong, K.M. (2007). Expression profiling defines a recurrence signature in lung squamous cell carcinoma. Carcinogenesis *28*, 760–766.

Li, T., Morgan, M.J., Choksi, S., Zhang, Y., Kim, Y.S., and Liu, Z.G. (2010). MicroRNAs modulate the noncanonical transcription factor NF-kappaB pathway by regulating expression of the kinase IKKalpha during macrophage differentiation. Nat. Immunol. *11*, 799–805.

Liang, J., Song, W., Tromp, G., Kolattukudy, P.E., and Fu, M. (2008a). Genome-wide survey and expression profiling of CCCH-zinc finger family reveals a functional module in macrophage activation. PLoS ONE *3*, e2880.

Liang, J., Wang, J., Azfer, A., Song, W., Tromp, G., Kolattukudy, P.E., and Fu, M. (2008b). A novel CCCH-zinc finger protein family regulates proinflammatory activation of macrophages. J. Biol. Chem. *283*, 6337–6346.

Lu, J., Getz, G., Miska, E.A., Alvarez-Saavedra, E., Lamb, J., Peck, D., Sweet-Cordero, A., Ebert, B.L., Mak, R.H., Ferrando, A.A., et al. (2005). MicroRNA expression profiles classify human cancers. Nature *435*, 834–838.

Martello, G., Rosato, A., Ferrari, F., Manfrin, A., Cordenonsi, M., Dupont, S., Enzo, E., Guzzardo, V., Rondina, M., Spruce, T., et al. (2010). A MicroRNA targeting dicer for metastasis control. Cell *141*, 1195–1207.

Matsushita, K., Takeuchi, O., Standley, D.M., Kumagai, Y., Kawagoe, T., Miyake, T., Satoh, T., Kato, H., Tsujimura, T., Nakamura, H., and Akira, S. (2009). Zc3h12a is an RNase essential for controlling immune responses by regulating mRNA decay. Nature *458*, 1185–1190.

Melo, S.A., Moutinho, C., Ropero, S., Calin, G.A., Rossi, S., Spizzo, R., Fernandez, A.F., Davalos, V., Villanueva, A., Montoya, G., et al. (2010). A genetic defect in exportin-5 traps precursor microRNAs in the nucleus of cancer cells. Cancer Cell *18*, 303–315.

Merritt, W.M., Lin, Y.G., Han, L.Y., Kamat, A.A., Spannuth, W.A., Schmandt, R., Urbauer, D., Pennacchio, L.A., Cheng, J.F., Nick, A.M., et al. (2008). Dicer, Drosha, and outcomes in patients with ovarian cancer. N. Engl. J. Med. *359*, 2641–2650.

Moschos, S.A., Williams, A.E., Perry, M.M., Birrell, M.A., Belvisi, M.G., and Lindsay, M.A. (2007). Expression profiling in vivo demonstrates rapid changes in lung microRNA levels following lipopolysaccharide-induced inflammation but not in the anti-inflammatory action of glucocorticoids. BMC Genomics *8*, 240.

Nagel, R., le Sage, C., Diosdado, B., van der Waal, M., Oude Vrielink, J.A., Bolijn, A., Meijer, G.A., and Agami, R. (2008). Regulation of the adenomatous polyposis coli gene by the miR-135 family in colorectal cancer. Cancer Res. *68*, 5795–5802.

O'Connell, R.M., Rao, D.S., Chaudhuri, A.A., and Baltimore, D. (2010). Physiological and pathological roles for microRNAs in the immune system. Nat. Rev. Immunol. *10*, 111–122.

Ozen, M., Creighton, C.J., Ozdemir, M., and Ittmann, M. (2008). Widespread deregulation of microRNA expression in human prostate cancer. Oncogene *27*, 1788–1793.

Paschoud, S., Dogar, A.M., Kuntz, C., Grisoni-Neupert, B., Richman, L., and Kühn, L.C. (2006). Destabilization of interleukin-6 mRNA requires a putative RNA stem-loop structure, an AU-rich element, and the RNA-binding protein AUF1. Mol. Cell. Biol. *26*, 8228–8241.

Ramachandran, V., and Chen, X. (2008). Degradation of microRNAs by a family of exoribonucleases in Arabidopsis. Science *321*, 1490–1492.

Rodriguez, A., Vigorito, E., Clare, S., Warren, M.V., Couttet, P., Soond, D.R., van Dongen, S., Grocock, R.J., Das, P.P., Miska, E.A., et al. (2007). Requirement of bic/microRNA-155 for normal immune function. Science *316*, 608–611.

Ruggiero, T., Trabucchi, M., De Santa, F., Zupo, S., Harfe, B.D., McManus, M.T., Rosenfeld, M.G., Briata, P., and Gherzi, R. (2009). LPS induces KH-type splicing regulatory protein-dependent processing of microRNA-155 precursors in macrophages. FASEB J. *23*, 2898–2908.

Sadler, A.J., and Williams, B.R. (2008). Interferon-inducible antiviral effectors. Nat. Rev. Immunol. *8*, 559–568.

Salehzada, T., Silhol, M., Steff, A.M., Lebleu, B., and Bisbal, C. (1993). 2′,5′-Oligoadenylate-dependent RNase L is a dimer of regulatory and catalytic subunits. J. Biol. Chem. *268*, 7733–7740.

Sandberg, R., Neilson, J.R., Sarma, A., Sharp, P.A., and Burge, C.B. (2008). Proliferating cells express mRNAs with shortened 3′ untranslated regions and fewer microRNA target sites. Science *320*, 1643–1647.

Shedden, K., Taylor, J.M., Enkemann, S.A., Tsao, M.S., Yeatman, T.J., Gerald, W.L., Eschrich, S., Jurisica, I., Giordano, T.J., Misek, D.E., et al; Director's Challenge Consortium for the Molecular Classification of Lung Adenocarcinoma. (2008). Gene expression-based survival prediction in lung adenocarcinoma: a multi-site, blinded validation study. Nat. Med. *14*, 822–827.

Siomi, H., and Siomi, M.C. (2010). Posttranscriptional regulation of microRNA biogenesis in animals. Mol. Cell *38*, 323–332.

Subramanian, A., Tamayo, P., Mootha, V.K., Mukherjee, S., Ebert, B.L., Gillette, M.A., Paulovich, A., Pomeroy, S.L., Golub, T.R., Lander, E.S., and Mesirov, J.P. (2005). Gene set enrichment analysis: a knowledge-based approach for interpreting genome-wide expression profiles. Proc. Natl. Acad. Sci. USA *102*, 15545–15550.

Suzuki, H.I., and Miyazono, K. (2010). Dynamics of microRNA biogenesis: crosstalk between p53 network and microRNA processing pathway. J. Mol. Med. *88*, 1085–1094.

Suzuki, H.I., and Miyazono, K. (2011). Emerging complexity of microRNA generation cascades. J. Biochem. *149*, 15–25.

Suzuki, H.I., Yamagata, K., Sugimoto, K., Iwamoto, T., Kato, S., and Miyazono, K. (2009). Modulation of microRNA processing by p53. Nature *460*, 529–533.

Umbach, J.L., and Cullen, B.R. (2009). The role of RNAi and microRNAs in animal virus replication and antiviral immunity. Genes Dev. *23*, 1151–1164.

Wu, H., Neilson, J.R., Kumar, P., Manocha, M., Shankar, P., Sharp, P.A., and Manjunath, N. (2007). miRNA profiling of naïve, effector and memory CD8 T cells. PLoS ONE *2*, e1020.

Xiao, C., Srinivasan, L., Calado, D.P., Patterson, H.C., Zhang, B., Wang, J., Henderson, J.M., Kutok, J.L., and Rajewsky, K. (2008). Lymphoproliferative disease and autoimmunity in mice with increased miR-17-92 expression in lymphocytes. Nat. Immunol. *9*, 405–414.

Zhang, H., Kolb, F.A., Jaskiewicz, L., Westhof, E., and Filipowicz, W. (2004). Single processing center models for human Dicer and bacterial RNase III. Cell *118*, 57–68.

Zuker, M. (2003). Mfold web server for nucleic acid folding and hybridization prediction. Nucleic Acids Res. *31*, 3406–3415.

Overexpression of enhancer of zeste homolog 2 with trimethylation of lysine 27 on histone H3 in adult T-cell leukemia/lymphoma as a target for epigenetic therapy

Daisuke Sasaki,[1] Yoshitaka Imaizumi,[2] Hiroo Hasegawa,[1] Akemi Osaka,[1] Kunihiro Tsukasaki,[2] Young Lim Choi,[3] Hiroyuki Mano,[3] Victor E. Marquez,[4] Tomayoshi Hayashi,[5] Katsunori Yanagihara,[1] Yuji Moriwaki,[2] Yasushi Miyazaki,[2] Shimeru Kamihira,[1] and Yasuaki Yamada[1]

[1]Department of Laboratory Medicine, Nagasaki University Graduate School of Biomedical Sciences, Nagasaki, Japan; [2]Department of Hematology and Molecular Medicine, Atomic Bomb Disease Institute, Nagasaki University Graduate School of Biomedical Sciences, Nagasaki, Japan; [3]Division of Functional Genomics, Jichi Medical University, Tochigi, Japan; [4]Chemical Biology Laboratory, National Cancer Institute, Frederick, MD, USA; and [5]Department of Pathology, Nagasaki University Hospital, Nagasaki, Japan

ABSTRACT

Background
Enhancer of zeste homolog 2 is a component of the Polycomb repressive complex 2 that mediates chromatin-based gene silencing through trimethylation of lysine 27 on histone H3. This complex plays vital roles in the regulation of development-specific gene expression.

Design and Methods
In this study, a comparative microarray analysis of gene expression in primary adult T-cell leukemia/lymphoma samples was performed, and the results were evaluated for their oncogenic and clinical significance.

Results
Significantly higher levels of Enhancr of zeste homolog 2 and RING1 and YY1 binding protein transcripts with enhanced levels of trimethylation of lysine 27 on histone H3 were found in adult T-cell leukemia/lymphoma cells compared with those in normal $CD4^+$ T cells. Furthermore, there was an inverse correlation between the expression level of Enhancer of zeste homolog 2 and that of miR-101 or miR-128a, suggesting that the altered expression of the latter miRNAs accounts for the overexpression of the former. Patients with high Enhancer of zeste homolog 2 or RING1 and YY1 binding protein transcripts had a significantly worse prognosis than those without it, indicating a possible role of these genes in the oncogenesis and progression of this disease. Indeed, adult T-cell leukemia/lymphoma cells were sensitive to a histone methylation inhibitor, 3-deazaneplanocin A. Furthermore, 3-deazaneplanocin A and histone deacetylase inhibitor panobinostat showed a synergistic effect in killing the cells

Conclusions
These findings reveal that adult T-cell leukemia/lymphoma cells have deregulated Polycomb repressive complex 2 with over-expressed Enhancer of zeste homolog 2, and that there is the possibility of a new therapeutic strategy targeting histone methylation in this disease.

Key words: adult T-cell leukemia/lymphoma, human T-cell leukemia virus type-1, Enhancer of zeste homolog 2, H3K27me3.

Citation: Sasaki D, Imaizumi Y, Hasegawa H, Osaka A, Tsukasaki K, Choi YL, Mano H, Marquez VE, Hayashi T, Yanagihara K, Moriwaki Y, Miyazaki Y, Kamihira S, and Yamada Y. Overexpression of enhancer of zeste homolog 2 with trimethylation of lysine 27 on histone H3 in adult T-cell leukemia/lymphoma as a target for epigenetic therapy Haematologica 2011;96(4):712-719. doi:10.3324/haematol.2010.028605

Funding: supported in part by a Grant-in-Aid for Scientific Research from the Ministry of Health, Labour, and Welfare of Japan (N. 04010119). For VEM, this research was supported in part by the Intramural Research Program of the NIH, Center for Cancer Research, NCI-Frederick.

Acknowledgments: the authors thank Sayaka Mori and Yuko Doi for excellent technical assistance.

Manuscript received June 16, 2010. Revised version arrived on December 16, 2010. Manuscript accepted on December 31, 2010.

Correspondence:
Yasuaki Yamada, Department of Laboratory Medicine, 1-7-1 Sakamoto, Nagasaki 852-8501, Japan. Phone: international +81.958197408.
Fax: international +81.958197422.
E-mail: y-yamada@nagasaki-u.ac.jp

The online version of this article has a Supplementary Appendix.

Introduction

The Polycomb group (PcG) proteins play critical roles in the regulation of development by repressing specific sets of developmental genes through chromatin modification.[1] They form two distinct multimeric complexes, Polycomb repressive complex 1 (PRC1) and PRC2, which bind to polycomb responsive elements (PRE), repress genes required for cell differentiation, and maintain pluripotency and self-renewal of embryonic stem cells and hematopoietic stem cells.[2,3] PRC2 consists of Enhancer of zeste homolog 2 (EZH2), which has histone methyltransferase activity, suppressor of zeste 12 (SUZ12), and embryonic ectoderm development (EED), which is required to maintain the integrity of PRC2.[1,4] Sequence-specific DNA binding protein YY1, which recognizes PRE, interacts with EED and recruits PRC2 to a specific chromatin domain to be repressed.[5] EED interacts with histone deacetylase (HDAC) proteins, HDAC1 and HDAC2, and the histone binding proteins RBBP4 (RbAp48) and RBBP7 (RbAp46).[6] PRC2 thus also participates in histone deacetylation. EZH2, as a part of the PRC2 complex, not only methylates histone but also serves as a recruitment platform for DNA methyltransferases that methylate the promoter regions of target genes, which is another mechanism of gene repression.[7] The more diverse complex PRC1 consists of HPC family proteins that mediate chromatin association, HPH family proteins, RING, BMI1, and others.[1] PRC2 initiates trimethylation of lysine 27 on histone H3 (H3K27me3) and, to a lesser extent, lysine 9 of histone H3.[8] PRC1 recognizes H3K27me3 through the chromodomain of the HPC and maintains the trimethylation. There are a number of reports indicating that such epigenetically mediated transcriptional silencing is associated with cancer development.[1,9] Among these, oncogenic roles of over-expressed EZH2 have been studied in a variety of tumors.[10]

Adult T-cell leukemia/lymphoma (ATL) is a neoplasm of mature CD4+ T-cell origin, etiologically associated with human T-cell leukemia virus type-1 (HTLV-1).[11,12] Its clinical behavior differs among patients and is subclassified into four subtypes: smoldering type and chronic type as indolent subtypes, and acute type and lymphoma type as aggressive subtypes.[13] Inactivation of tumor suppressor genes is one of the key events in development and progression, and there is a strong accumulation of *p14ARF/p15INK4B/p16INK4A* gene deletion/methylation or *p53* gene mutations in aggressive subtypes (>60%).[14-20] In the present study, for further investigation of the oncogenesis of ATL, we performed a comparative microarray analysis of gene expression in primary ATL samples. ATL cells expressed significantly higher levels of *EZH2* and *RYBP* (RING1 and YY1 binding protein) transcripts than CD4+ T cells from healthy volunteers. Moreover, acute-type ATL cells showed significantly higher levels of these transcripts than chronic-type ATL cells, suggesting that deregulation of PcG proteins plays a crucial role not only in the development but also in the progression of ATL. In addition, ATL samples were strongly positive for H3K27me3, and were sensitive to 3-deazaneplanocin A (DZNep), a histone methylation inhibitor.[21-23] It has recently been shown that HDAC inhibitor panobinostat (PS, also known as LBH589) depletes the levels of EZH2, SUZ12, and EED and induces apoptotic death in leukemia cells.[24] Deregulation of PcG protein genes with over-expressed EZH2 in ATL cells suggests that ATL is one of the appropriate target diseases for such epigenetic therapy.

Design and Methods

Sample preparation

This study was approved by the ethics committees of Nagasaki University, and all clinical samples were obtained after written informed consent was provided. The diagnosis of ATL was confirmed by the monoclonal integration of HTLV-1 proviral DNA in the genomic DNA of leukemia cells. Peripheral blood mononuclear cells (PBMCs) were obtained from ATL patients (acute type 22 cases, chronic type 19 cases) and healthy adult volunteers by density gradient centrifugation using Lympho-prep (AXIS SHIELD, Oslo, Norway). For enrichment of ATL cells, CD4+ cells were purified from the PBMCs by the magnetic bead method (CD4 MicroBeads, Miltenyi Biotec, Auburn, CA, USA) as described elsewhere.[25] Besides these samples for microarray analysis, we prepared another set of samples for quantitative real-time RT-PCR (qRT-PCR) and Western blotting (25 ATL patients, 13 HTLV-1 carriers, and 12 healthy adults) to confirm the results of microarray analysis. We also used formalin-fixed, paraffin-embedded lymph nodes from 7 patients with lymphoma-type ATL and 5 patients with follicular lymphoma for immunohistochemical analysis.

ATL cell lines used in this study, SO4, ST1, KK1, KOB, and LM-Y1, were established from respective patients in our laboratory and have been confirmed to be of primary ATL cell origin.[26] Cells were maintained in RPMI1640 medium supplemented with 10% FBS and 100 Japan reference units of recombinant interleukin-2 (rIL-2) (kindly provided by Takeda Pharmaceutical Company, Ltd., Osaka, Japan). We also used HTLV-1-infected T-cell lines MT2 and HuT102 and acute T-lymphoblastic leukemia cell lines Jurkat and MOLT4, which were maintained without rIL-2.

DNA microarray analysis

RNA was prepared from purified CD4+ T cells, and subjected to hybridization to HGU133A & B microarray containing 44,760 probe sets for human genes (Affymetrix, Santa Clara, CA, USA) as described previously.[25,27] The mean expression intensity of the internal positive control probe sets (*http://www.affymetrix.com/support/technical/mask_files.affx*) was set to 500 units in each hybridization, and the fluorescence intensity of each test gene was normalized accordingly. All HGU133A & B microarray data are available from the Gene Expression Omnibus website (*http://www.ncbi.nlm.nih.gov/geo*) under the accession number GSE1466.

Quantitative real-time RT-PCR

For confirmation of the results of microarray analysis, we performed quantitative real-time RT-PCR (qRT-PCR) for PcG protein genes. Total RNA was prepared using Isogen (Wako, Osaka, Japan). After removal of contaminated DNA with DNase (Message Clean kit; GenHunter, Nashville, TN, USA), cDNA was constructed from 1 μg of total RNA using the SuperScript III RT-PCR System (Invitrogen, Carlsbad, CA, USA) according to the manufacturer's instructions. Primers and TaqMan probes labeled with TAMRA dye at the 3' end and FAM at the 5' end are listed in *Online Supplementary Table S1*. The mRNA levels for PcG family proteins and porphobilinogen deaminase (PBGD) were measured from a cDNA template using a LightCycler480 PCR System (Roche Diagnostics, Mannheim, Germany). Briefly, reactions were performed in a 20 μL volume with 5 μL (25 ng) of cDNA, 0.5 μM PCR primers, 0.1 μM TaqMan probes, and 10 μL of LightCycler

480 probes Master Mix (Roche Diagnostics). The PCR program consisted of 95°C for 5 min followed by 50 cycles of 95°C for 10 sec and 60°C for 30 sec. After 50 cycles, the absolute amounts of PcG protein mRNA and *PBGD* mRNA were interpolated from the standard curves generated by the dilution method using plasmids derived from a clone transfected with pTAC-1 Vector (BioDynamics Laboratory Inc., Tokyo, Japan) containing amplicons from the PcG family protein and PBGD genes, respectively. To normalize these results for variability in concentration and integrity of RNA and cDNA, the *PBGD* gene was used as an internal control in each sample.

For the quantitative PCR for microRNAs (miRNAs), miR-101, miR-26a, and miR-128a, 10 ng of total RNA (containing miRNA) was used. RT reaction and real-time quantification were performed using TaqMan MicroRNA RT kit and TaqMan MicroRNA assays (hsa-miR-26a, assay ID 000405; hsa-miR-101, assay ID 002253; hsa-miR-128a, assay ID 002216; RNU6B, assay ID 001093) (Applied Biosystems, Foster City, CA, USA) in accordance with the manufacturer's instructions. Each PCR reaction mixture contained 10 μL of LightCycler 480 probes Master Mix, 4 μL of nuclease-free water, 1 μL of 20X specific PCR primer, and 5 μL of RT product. The thermal cycler was programmed as follows: 95°C for 5 min, 40 cycles of 95°C for 15 sec, and 60°C for 60 sec. Using the comparative CT method, we used an endogenous control (RNU6B) to normalize the expression levels of target micro-RNA by correcting differences in the amount of RNA loaded into qPCR reactions.

Western blot analysis and antibodies

Western blot analysis was performed as described previously.[28] The analysis was performed using antibodies to EZH2 and Histone H3 (Cell Signaling Technology, Danvers, MA, USA), phospho EZH2 (Ser21) (Bethyl Laboratories, Montgomery, TX, USA), H3K27me3, dimethylated H3K27 (H3K27me2), monomethylated H3K27 (H3K27me1) (Millipore, Temecula, CA, USA), and β-actin (Sigma, St. Louis, MO, USA).

Immunohistochemistry

Immunohistochemical staining for EZH2 and H3K27me3 was performed on formalin-fixed, paraffin-embedded lymph node samples from lymphoma-type ATL patients and follicular lymphoma patients as a control. The deparaffinized slides were pretreated with DAKO Target Retrieval Solution, pH 9 (DAKO Japan, Tokyo, Japan), and heated in a water bath at 95°C for 40 min. For all stains, the endogenous peroxidase was quenched using 3% H_2O_2 for 15 min. Sections were then placed in 0.5% non-fat dry milk for 30 min at room temperature. The primary antibodies used were anti-EZH2 antibody (BD Biosciences, San Jose, CA, USA) and anti-H3K27me3 antibody (Cell Signaling Technology, Boston, MA, USA), and were applied at 1:50 dilution and 1:100 dilution, respectively. They were allowed to react for 1 h at room temperature, and then the DAKO EnVision™ + Dual Link System-HRP (DAKO Japan, Tokyo, Japan) was applied using diaminobenzidine as the chromogen, following the manufacturer's protocol.

Sensitivity of adult T-cell leukemia/lymphoma cell lines to DZNep and PS (LBH589)

DZNep was synthesized by one of the authors (VEM). Cells were treated with different concentrations of DZNep for 72 h and the cell proliferation status was evaluated by an MTS assay using a Cell Titer 96® AQueos Cell Proliferation Assay kit (Promega, Madison, WI, USA) in accordance with the manufacturer's instructions. To analyze the synergistic effect of combined treatment with DZNep and PS (LBH589) (kindly provided by Novartis Pharma AG, Basel, Switzerland), cells were treated with DZNep (0.3-5.0 μM) and PS (LBH589) (3-50 nM) for 48 h. After the cell proliferation status was evaluated by an MTS assay, the combination index (CI) for each drug combination was obtained by determining the median dose effect of Chou and Talalay using the CI equation within the commercially available software Calcusyn (Biosoft).[29] CI<1, CI=1, and CI>1 indicate synergism, additive effect, and antagonism, respectively. Cell viability represents the value relative to that of the control culture without these agents.

Results

Microarray analysis shows increased EZH2 and/or RYBP transcripts in adult T-cell leukemia/lymphoma cells

In a comparative microarray analysis of primary ATL samples, we focused on investigating PcG protein genes, *EZH2*, *RYBP*, *BMI-1*, and *CBX7*, in the present study because ATL cells show many aberrantly hypermethylated DNA sequences.[30] ATL cells expressed significantly higher levels of *EZH2* and *RYBP* transcripts than $CD4^+$ T cells from healthy adults (Figure 1A and B). In addition, there was a difference between ATL subtypes in these expressions, and cells from the acute type showed significantly higher levels of these transcripts than the cells from the chronic type. When patients were separated into two groups consisting of those with high expression and those with low expression, the group with high *EZH2* or high *RYBP* transcript showed significantly shorter survival than the respective low-expression groups (Figure 1E and F), indicating that high *EZH2* and/or *RYBP* expression is associated with aggressive clinical behavior. Convincingly, there was a trend toward accumulation of acute-type ATL in the high *EZH2* or the high *RYBP* expression group: 14 cases of acute type and 6 cases of chronic type in the high *EZH2* group, 7 cases of acute type and 13 cases of chronic type in the low *EZH2* group, 14 cases of acute type and 6 cases of chronic type in the high RYBP group, and 7 cases of acute type and 13 cases of chronic type in the low RYBP group. BMI1 is known to down-regulate the expression of *p14ARF/p16INK4A* and lead to neoplastic transformation.[31] Chromobox 7 (CBX7), a component of the PRC1, is also known to repress the transcription of *p14ARF/p16INK4A*.[32] Since inactivation of *p14ARF/p15INK4B/p16INK4A* genes is one of the key events in ATL progression, expression of *BMI-1* and/or *CBX7* transcript was expected to be elevated in acute-type ATL cells. There was, however, no difference in these expressions between ATL subtypes or even between ATL cells and normal $CD4^+$ T cells (Figure 1C and D). There was no difference in survival for different *BMI-1* or *CBX7* expression levels (Figure 1G and H).

Confirmation of increased EZH2 and/or RYBP transcripts by quantitative real-time RT-PCR

For confirmation of the results of microarray analysis, we quantified the transcripts of the PcG protein genes including *EZH2* and *RYBP* by qRT-PCR using another set of samples from ATL patients, healthy adults, HTLV-1 carriers, and hematologic cell lines including ATL cell lines. In accordance with the results of microarray analysis, *EZH2* and *RYBP* transcripts were increased in primary ATL cells compared with those in the cells from healthy adults and HTLV-1 carriers, with statistically significantly higher val-

ues in *EZH2* in terms of both absolute copy number per 25 ng of total RNA and normalized expression level (*Online Supplementary Figure S1A, a, B, b*). *RBBP4* was significantly higher in primary ATL cells than in the cells from healthy adults and HTLV-1 carriers in terms of normalized expression level (*Online Supplementary Figure S1 C, c*). In contrast, there was no difference in *BMI1*, *YY1*, and *EED* expressions among these groups, although some patients showed very high *BMI1* expression (*Online Supplementary Figure S1D, d, E, e, F, f*). Similarly to primary ATL cells, some ATL cell lines showed high *EZH2* expression in terms of absolute copy number per 25 ng of total RNA (*Online Supplementary Figure S1A*).

EZH2 protein expression with trimethylation of H3K27 is characteristic in adult T-cell leukemia/lymphoma cells

We then examined EZH2 and RYBP at the protein level by Western blotting. A 98-kDa band for EZH2 protein and a 32-kDa band for RYBP protein were detected in all primary ATL samples irrespective of subtype, but they were hardly detected in cells from healthy adults and HTLV-1 carriers (Figure 2A, *Online Supplementary Figure S2*, and *data not shown*). ATL cell lines and acute T-lymphoblastic leukemia cell lines also showed intense EZH2 bands. The serine-threonine kinase Akt phosphorylates EZH2 at serine 21 and suppresses its methyltransferase activity by impeding EZH2 binding to histone H3, which results in a decrease in lysine 27 trimethylation.[33] EZH2 of ATL cells was not phosphorylated and was in its active form (Figure 2A). In fact, most primary ATL samples showed the band for H3K27me3, while the cells from healthy adults lacked the band (Figure 2B). As it is known that EZH2 plays a crucial role in trimethylation but not in dimethylation or monomethylation, the bands for H3K27me2 and H3K27me1 were detected in all samples examined, but the band for H3K27me3 was limited in primary ATL cells and ATL cell lines LMY1 and KOB that showed an intense EZH2 band with a faint phosphorylated EZH2 band (Figure 2A and B). In contrast, EZH2 was strongly phosphorylated in ATL cell lines ST1, SO4, KK1, and acute T-lymphoblastic leukemia cell lines Jurkat and MOLT4, and these cell lines hardly showed the band for H3K27me3. Collectively, these results indicate that ATL cells express

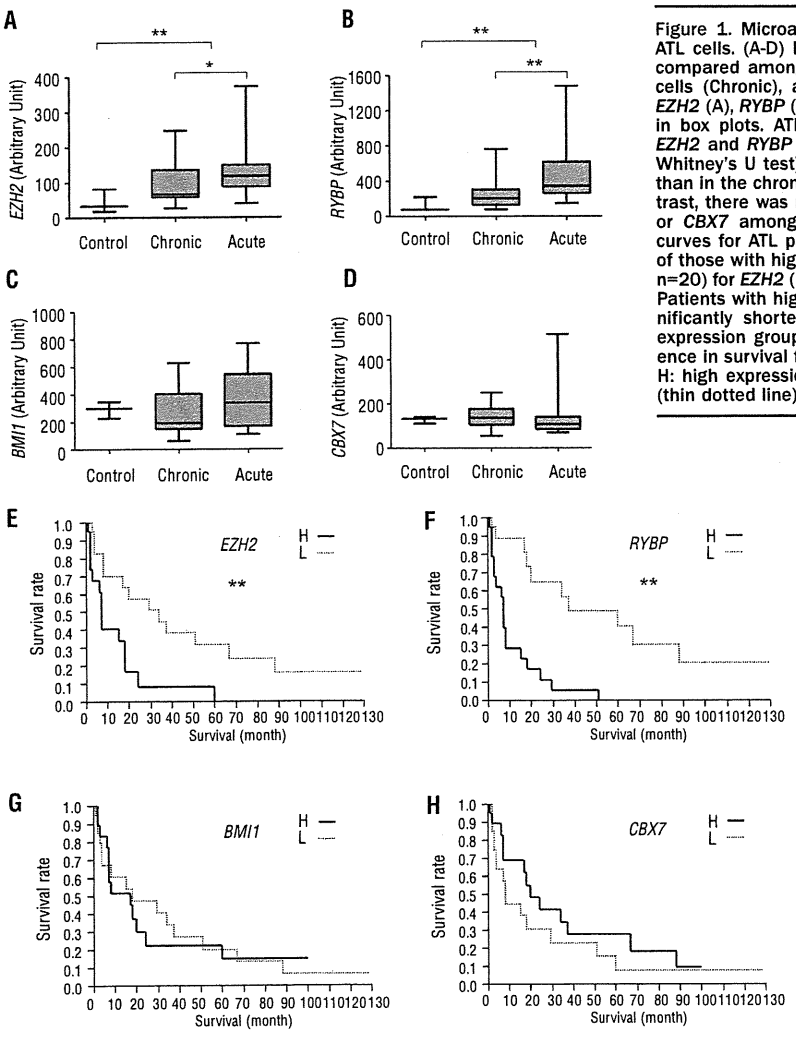

Figure 1. Microarray analysis of gene expression in primary ATL cells. (A-D) Expression levels of PcG protein genes were compared among normal CD4+ T cells (Control), chronic ATL cells (Chronic), and acute ATL cells (Acute), and results of *EZH2* (A), *RYBP* (B), *BMI1* (C), and *CBX7* (D) are demonstrated in box plots. ATL cells showed significantly higher levels of *EZH2* and *RYBP* transcripts than normal CD4+ T cells (Mann-Whitney's U test), with a higher expression in the acute type than in the chronic type (Mann-Whitney's U test) (A, B). In contrast, there was no statistical difference in the level for *BMI1* or *CBX7* among these groups (C, D). (E-H) Overall survival curves for ATL patients separated into two groups consisting of those with high expression (H, n=20) and low expression (L, n=20) for *EZH2* (E), *RYBP* (F), *BMI1* (G), or *CBX7* (H) are shown. Patients with high *EZH2* or high *RYBP* expression showed significantly shorter survival than those in corresponding low expression groups (log rank test) (E, F). There was no difference in survival for different *BMI1* or *CBX7* expressions (G, H). H: high expression group (bold line), L: low expression group (thin dotted line). $*P<0.05$, $**P<0.01$

functionally active EZH2, and as a result, their H3K27 are trimethylated, and that ATL cell lines LMY1 and KOB preserve this characteristic of primary ATL cells.

Immunohistochemical confirmation of the expression of EZH2 and H3K27me3 in lymph nodes

We next used lymph nodes from lymphoma-type ATL patients for immunohistochemical evaluation of EZH2 expression and H3K27me3. In agreement with the results of Western blotting, all ATL lymph nodes from 7 patients were strongly positive for both EZH2 and H3K27me3 without exception in their nuclear staining (*Online Supplementary Figure S3* and *data not shown*), suggesting that overexpression of EZH2 with H3K27me3 is a common feature of ATL cells irrespective of ATL subtypes. In contrast, in lymph nodes from 5 follicular lymphoma patients, only a few cells were positive for EZH2 with some variation among patients and most cells were negative for H3K27me3 (*Online Supplementary Figure S3* and *data not shown*).

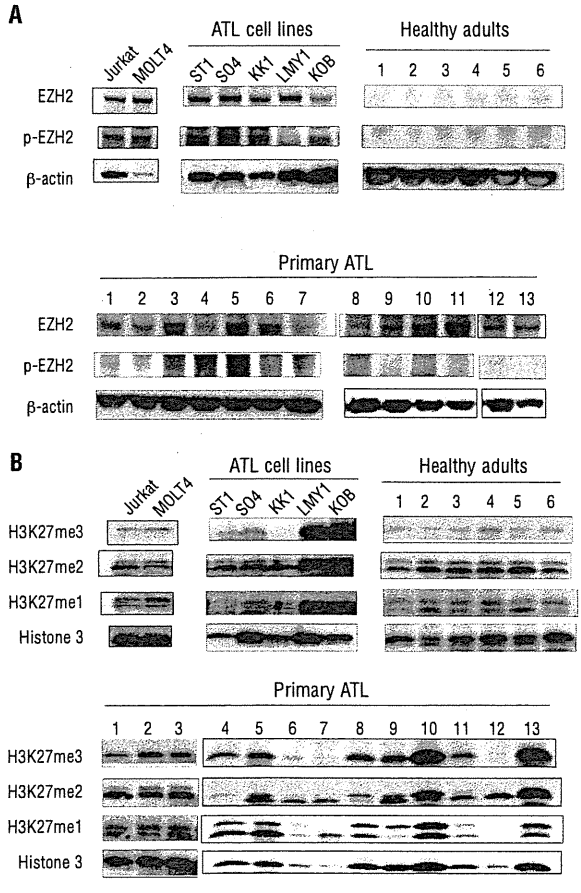

Figure 2. EZH2 protein expression and histone methylation. (A) Western blot analysis for EZH2 protein was performed on primary ATL cells, cells from healthy adults, and ATL cell lines. Primary ATL cells showed a clear 98-kDa band for EZH2 with the absence or presence of faint bands for phosphorylated EZH2 (p-EZH2). Cells from healthy adults hardly showed these bands. ATL cell lines ST1, SO4, and KK1 showed intense bands for both EZH2 and p-EZH2, but LM-Y1 and KOB cells showed intense bands for EZH2 with the absence of a band for p-EZH2. (B) Western blot analysis for histone methylation status was performed. Only primary ATL cells and LM-Y1 and KOB cell lines showed a clear band for H3K27me3, but others hardly showed the band. Bands for H3K27me2, H3K27me1, and histone H3 were observed in almost all samples examined.

Downregulation of miR-101 and miR-128a may be responsible for increased EZH2 expression

So far, more than 700 miRNAs have been identified in humans, and each miRNA regulates multiple target genes. miR-101 and miR-26a have been shown to be negative regulators of *EZH2* expression and are depressed in several types of cancer cells.[34,35] miR-128a is known to be a negative regulator of *BMI1* and has been reported to be involved in glioma cell proliferation.[36] We quantified these miRNAs in primary ATL cells and cells from HTLV-1 carriers to investigate the mechanism of *EZH2* overexpression. ATL cells showed significantly decreased levels of miR-101 and miR-128a compared with the cells from HTLV-1 carriers (Figure 3A and C). Notably, there were significant inverse correlations between *EZH2* expression and miR-101 expression or *EZH2* expression and miR-128a expression (Figure 3D and E), suggesting that decrease of these miRNAs accounts for the overexpression of *EZH2*. Since genomic loss of miR-101 has been reported in prostate cancer,[34] we performed quantitative genomic PCR for miR-101 in two loci, miR-101-1 (chromosome 1p31) and miR-101-2 (chromosome 9p24). Both loci were preserved in all 10 ATL samples examined (*Online Supplementary Figure S4*). The expression of miR-26a did not, in contrast, differ between ATL cells and cells from HTLV-1 carriers (Figure 3B). Unexpectedly, there was no significant correlation between *BMI1* expression and miR-128a expression (Figure 3F).

Adult T-cell leukemia/lymphoma cells are sensitive to DZNep and PS (LBH589)

We first examined the sensitivity of ATL-related cell lines and acute T-lymphoblastic leukemia cell lines to DZNep, an inhibitor of S-adenosylhomocysteine hydrolase, which has recently been shown to decrease the expression of EZH2 and histone methylation.[22,23] DZNep inhibited the proliferation of these cell lines, at concentrations above 0.5 μM (*Online Supplementary Figure S5A*). In contrast, $CD4^+$ T cells from healthy adults as a normal control were resistant to DZNep even at 5 μM. Notably, although DZNep decreased *EZH2* expression in ST1, SO4, and KK1, it did not decrease but rather increased the expression in KOB, results which were confirmed by Western blot (*Online Supplementary Figure S5B and C*). PS (LBH589) is also known to decrease the level of EZH2 in several types of leukemia cells.[24] One hundred nM of PS (LBH589) decreased *EZH2* expression at both transcript and protein levels in ATL cell lines including KOB and LM-Y1, which showed a similar EZH2 expression profile to that of primary ATL cells, namely, high EZH2 expression with low phosphorylated EZH2 and strong H3K27me3 (*Online Supplementary Figure S5D and E*). We next examined whether these agents show a synergistic effect or just an additive effect. As shown in *Online Supplementary Figure S5F* (upper panel), the cell viabilities of LM-Y1 treated with 25 nM PS (LBH589) or 2.5 μM DZNep were 70% and 87%, respectively. A combination of this setting (LBH:DZNep=1:100) markedly decreased the proportion of viable cells (40%) compared with that of cells treated

with either agent alone. Similarly, cell viabilities of KOB treated with 25 nM PS (LBH589), 2.5 μM DZNep, or a combination of these agents were 86%, 93%, and 48%, respectively. By calculating CI according to the method of Chou and Talalay,[29] we found a strong synergistic antiproliferative effect in both cell lines (*Online Supplementary Figure S5F*, lower panel).

Discussion

EZH2 is a critical component of PRC2, which mediates epigenetic gene silencing through trimethylation of H3K27.[37,38] EED and SUZ12 are also required for the exhibition of methyltransferase activity and for the localization of this complex to target genes.[39] In an analysis of genome-wide H3K27 methylation in aggressive prostate cancer tissues, a significant subset of the target genes were also targets in embryonic stem cells, suggesting that the mechanism for gene silencing used to maintain stem cell renewal is converted into oncogenesis.[40] Ectopic expression of EZH2 is capable of providing a proliferative advantage to primary cells, and its gene locus is amplified in primary tumors.[41] Indeed, increased EZH2 expression has been reported in several types of cancer cells, and its clinical significance is extensively studied in prostate cancer.[42] Amounts of both *EZH2* transcript and EZH2 protein were elevated in metastatic prostate cancer; in addition, clinically localized prostate cancers that express higher concentrations of *EZH2* showed a poorer prognosis. An association of increased EZH2 expression with poor prognosis has also been reported in other solid tumors. Currently, however, there are only limited reports describing EZH2 expression in hematologic malignancies.

In the present study, we showed for the first time that EZH2 was over-expressed in ATL cells, and that the increased EZH2 was not phosphorylated and was in its active form. The increased EZH2 seemed to exhibit histone methyltransferase activity *in vivo*, as supported by the results that ATL cells from both peripheral blood and lymph nodes were strongly positive for H3K27me3. Since EZH2 was almost undetectable in cells from healthy adults and HTLV-1 carriers, it is likely that deregulation of PRC2 caused by over-expressed EZH2 is involved in the early steps of ATL oncogenesis. Meanwhile, ATL patients with high EZH2 expression showed shorter survival than patients with low EZH2 expression, indicating that increased EZH2 also plays a role in the process of ATL progression. It has been reported that genes methylated in cancer cells are specifically packaged with nucleosomes containing H3K27.[43] However, there are only a few studies that actually examined H3K27me3 in primary tumor cells or tissues. In one such study, H3K27me3 expression was unexpectedly lower in breast, ovarian, and pancreatic cancers than in corresponding normal tissues, although it has been reported that there are increased levels of H3K27me3 in breast cancer cell lines.[44,45] We do not have an adequate explanation for these conflicts at present, but there may be some differences in the process of oncogenesis between solid tumors and hematologic malignancies.

The mechanism of the overexpression of EZH2 in tumors remains largely unknown. miRNAs regulate gene expression and play important roles in cellular differentiation and embryonic stem cell development. Recently, two miRNAs, miR-101 and miR-26a, were found to repress *EZH2* expression. The expression of miR-101 decreases in parallel with an increase in *EZH2* expression during progression in prostate tumors.[34] In addition to these miRNAs, we examined miR-128a, which has been shown to repress *BMI1* expression in glioblastoma, because overexpression of *BMI-1* is associated with the development of malignant lymphoma.[31,36] ATL cells showed a decreased level of miR-

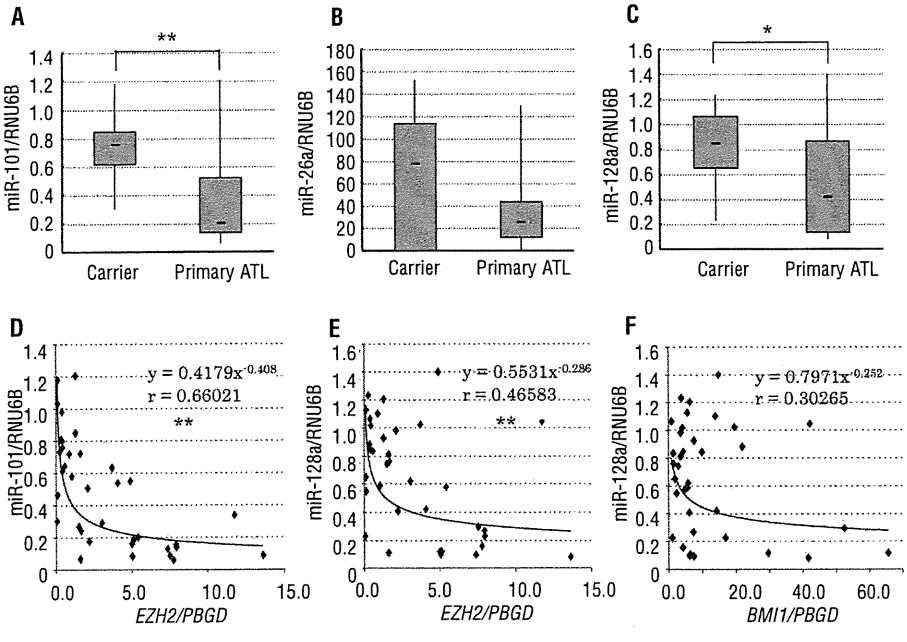

Figure 3. Quantitative real-time RT-PCR for miRNAs. (A-C) Expressions of miR-101 (A), miR-26a (B), and miR-128a (C) were compared between ATL patients and HTLV-1 carriers. Primary ATL cells showed significantly lower levels of miR-101 and miR-128a (Mann-Whitney's U test) compared with the cells from HTLV-1 carriers (A, C). There was no significant difference in miR-26a expression between the two groups (B). (D, E, F) Correlation between miRNA and *EZH2* or *BMI1* expression was examined. There were significant inverse correlations between normalized *EZH2* expression and miR-101 expression (D) or between normalized *EZH2* expression and miR-128a expression (E) (Spearman's correlation coefficient). In contrast, there was no correlation between normalized *BMI1* expression and miR-128a expression (F). *$P<0.05$, **$P<0.01$

101 expression compared with the cells from HTLV-1 carriers, which is not caused by genomic loss of the *miR-101* gene, in contrast to prostate cancer.[34] Moreover, there was a clear inverse correlation between *EZH2* expression and miR-101 expression, suggesting that increased *EZH2* is caused by the decrease in miR-101 expression. Although currently there is no report indicating an association of miR-128a with *EZH2* expression, miR-128a showed exactly the same pattern as miR-101, suggesting that the decrease in miR-128a also participates in *EZH2* overexpression in ATL. By analyzing the 3'-UTR sequence of *EZH2*, it has recently been shown that there are two predicted miR-101 target sites and one predicted miR-26a target site in the 3'-UTR of EZH2.[46] We performed a similar analysis and found that there was also a potential target site for miR-128a near one of the miR-101 target sites (*Online Supplementary Figure S6*). miR-26a was not decreased in ATL cells, and there was no correlation between miR-26a expression and *EZH2* expression or miR-128a expression and *BMI1* expression. The association of miR-26a with *EZH2* was found in normal cell differentiation as a physiological phenomenon but not in tumor cells. The miRNAs used to regulate normal development and differentiation may be different from those used for the development of tumors. Another possible explanation for the mechanism of increased *EZH2* expression in ATL is inactivation of *p14ARF/p15INK4B/p16INK4A* tumor suppressor genes, which frequently occurs in ATL.[14,15,19,20] EZH2 is a molecule downstream of the pRB-E2F pathway, and inactivation of these genes allows E2F to be released from pRB, which results in the upregulation of *EZH2* expression.[41] Several recent reports indicate that EZH2 functions to repress the expression of *p14ARF/p15INK4B/p16INK4A*; therefore, increased EZH2 may be used to further decrease the expression of *p14ARF/p15INK4B/p16INK4A*.[47] Since somatic mutations altering EZH2 (Tyr641) have recently been reported in follicular and diffuse large B-cell lymphomas of germinal-center origin,[48] we performed a similar analysis in 10 primary ATL samples. There were however no such mutations (*Online Supplementary Figure S7*).

ATL is quite resistant to antineoplastic agents and the median survival time of those with the aggressive subtypes is only 13 months, even in a recent multicenter clinical trial.[49] Since high EZH2 expression with H3K27me3 seems to be an essential component for the initiation and promotion of cell proliferation in ATL, we searched for the possibility of therapeutic strategies targeting EZH2. We examined the sensitivity of ATL cells to agents that have been shown to inhibit *EZH2* expression and histone methylation. DZNep is a carbocyclic analog of adenosine synthesized more than 20 years ago as an inhibitor of S-adenosylhomocysteine hydrolase, which has therapeutic potential as an anticancer or antiviral drug.[21] DZNep has recently aroused interest for its unique features; it decreases the expressions of *EZH2*, *SUZ12*, and *EED* with inhibition of H3K27 methylation and induces apoptosis in cancer cells but not in normal cells.[22,23] ATL cell lines were sensitive to DZNep and their cell proliferation was attenuated at one-tenth of the concentration used in these studies. More interestingly, DZNep showed no toxicity to normal $CD4^+$ T cells as a normal control. Acute T-lymphoblastic leukemia cell lines showed similar sensitivities to DZNep, which may indicate that DZNep exerts general toxicity to leukemia and lymphoma cells not necessarily associated with histone modification. Indeed, although DZNep rather increased EZH2 expression in KOB cells, this cell line was equally sensitive as other cell lines to DZNep. HDAC inhibitor PS (LBH589) is an effective agent for cutaneous T-cell lymphoma and induced complete remission in 2 of 9 patients involved in a phase I clinical trial.[50] More interestingly, it has been reported recently that combined use of DZNep and PS (LBH589) yielded more depletion of EZH2 and induced more apoptosis of leukemia cells, but not normal CD34 (+) bone marrow progenitor cells.[51] In the present study, we showed that the combination of DZNep and PS (LBH589) exhibited a synergistic effect in killing ATL cells. Thus, epigenetic therapy by the combined use of these agents that inhibit histone methylation could lead to a breakthrough in the treatment of aggressive ATL.

Authorship and Disclosures

The information provided by the authors about contributions from persons listed as authors and in acknowledgments is available with the full text of this paper at www.haematologica.org.

Financial and other disclosures provided by the authors using the ICMJE (www.icmje.org) Uniform Format for Disclosure of Competing Interests are also available at www.haematologica.org.

References

1. Sparmann A, van Lohuizen M. Polycomb silencers control cell fate, development and cancer. Nat Rev Cancer. 2006;6(11):846-56.
2. Lee TI, Jenner RG, Boyer LA, Guenther MG, Levine SS, Kumar RM, et al. Control of developmental regulators by Polycomb in human embryonic stem cells. Cell. 2006;125(2):301-13.
3. Kamminga LM, Bystrykh LV, de Boer A, Houwer S, Douma J, Weersing E, et al. The Polycomb group gene Ezh2 prevents hematopoietic stem cell exhaustion. Blood. 2006;107(5):2170-9.
4. van Lohuizen M, Tijms M, Voncken JW, Schumacher A, Magnuson T, Wientjens E. Interaction of mouse polycomb-group (Pc-G) proteins Enx1 and Enx2 with Eed: Indication for separate Pc-G complexes. Mol Cell Biol. 1998;18(6):3572-9.
5. Satijn DP, Hamer KM, den Blaauwen J, Otte AP. The Polycomb group protein EED interacts with YY1, and both proteins induce neural tissue in Xenopus embryos. Mol Cell Biol. 2001;21(4):1360-9.
6. van der Vlag J, Otte AP. Transcriptional repression mediated by the human polycomb-group protein EED involves histone deacetylation. Nat Genet. 1999;23(4):474-8.
7. Vire E, Brenner C, Deplus R, Blanchon L, Fraga M, Didelot C, et al. The Polycomb group protein EZH2 directly controls DNA methylation. Nature. 2006;439(7078):871-4.
8. Cao R, Zhang Y. The functions of E(Z)EZH2-mediated methylation of lysine 27 in histoneH3. Curr Opin Genet Dev. 2004;14(2):155-64.
9. Widschwendter M, Fiegl H, Egle D, Mueller-Holzner E, Spizzo G, Marth C, et al. Epigenetic stem cell signature in cancer. Nat Genet. 2007;39(2):157-8.
10. Simon JA, Lange CA. Roles of the EZH2 histone methyltransferase in cancer epigenetics. Mutat Res. 2008;647(1-2):21-9.
11. Uchiyama T, Yodoi J, Sagawa K, Takatsuki K, Uchino H. Adult T-cell leukemia: clinical and hematologic features of 16 cases. Blood. 1977;50(3):481-92.
12. Yoshida M, Seiki M, Yamaguchi K, Takatsuki K. Monoclonal integration of human T-cell leukemia provirus in all primary tumors of adult T-cell leukemia suggests causative role of human T-cell leukemia virus in the disease. Proc Natl Acad Sci USA. 1984;81(8):2534-7.
13. Shimoyama M and members of the Lymphoma Study Group (1984-1987):

Diagnostic criteria and classification of clinical subtypes of adult T-cell leukaemia-lymphoma. A report from the Lymphoma Study Group (1984-1987). Br J Haematol. 1991;79(3):428-37.
14. Hatta Y, Hirama T, Miller CW, Yamada Y, Tomonaga M, Koeffler HP. Homozygous deletions of p15 (MTS2) and p16 (CDKN2/MTS1) genes in adult T-cell leukemia. Blood. 1995;85(10):2699-704.
15. Yamada Y, Hatta Y, Murata K, Sugawara K, Ikeda S, Mine M, et al. Deletions of p15 and/or p16 genes as a poor-prognosis factor in adult T-cell leukemia. J Clin Oncol. 1997;15(5):1778-85.
16. Nagai H, Kinoshita T, Imamura J, Murakami Y, Hayashi K, Mukai K, et al. Genetic alteration of p53 in some patients with adult T-cell leukemia. Jpn J Cancer Res. 1991;82(12):1421-7.
17. Sakashita A, Hattori T, Miller CW, Suzushima H, Asou N, Takatsuki K, et al. Mutations of the p53 gene in adult T-cell leukemia. Blood. 1992;79(2):477-80.
18. Tawara M, Hogerzeil SJ, Yamada Y, Takasaki Y, Soda H, Hasegawa H, et al. Impact of p53 aberration on the progression of adult T-cell leukemia/lymphoma. Cancer Lett. 2006;234(2):249-55.
19. Kohno T, Yamada Y, Tawara M, Takasaki Y, Kamihira S, Tomonaga M, et al. Inactivation of p14ARF as a key event for the progression of adult T-cell leukemia/lymphoma. Leuk Res. 2007;31(12):1625-32.
20. Nosaka K, Maeda M, Tamiya S, Sakai T, Mitsuya H, Matsuoka M. Increasing methylation of the CDKN2A gene is associated with the progression of adult T-cell leukemia. Cancer Res. 2000;60(4):1043-8.
21. Glazer RI, Hartman KD, Knode MC, Richard MM, Chiang PK, Tseng CK, et al. 3-Deazaneplanocin: a new and potent inhibitor of S-adenosylhomocysteine hydrolase and its effects on human promyelocytic leukemia cell line HL-60. Biochem Biophys Res Commun. 1986;135 (2):688-94.
22. Miranda TB, Cortez CC, Yoo CB, Liang G, Abe M, Kelly TK, et al. DZNep is a global histone methylation inhibitor that reactivates developmental genes not silenced by DNA methylation. Mol Cancer Ther. 2009;8(6):1579-88.
23. Tan J, Yang X, Zhuang L, Jiang X, Chen W, Lee PL, et al. Pharmacologic disruption of Polycomb-repressive complex 2-mediated gene repression selectively induces apoptosis in cancer cells. Genes Dev. 2007;21(9): 1050-63.
24. Fiskus W, Pranpat M, Balasis M, Herger B, Rao R, Chinniyan A, et al. Histone deacetylase inhibitors deplete EZH2 and associated Polycomb Repressive Complex 2 proteins with attenuation of HOXA9 and MEIS1 and loss of survival of human acute leukemia cells. Mol Cancer Ther. 2006;5 (12):3096-104.
25. Choi YL, Tsukasaki K, O'Neill MC, Yamada Y, Onimaru Y, Matsumoto K, et al. A genomic analysis of adult T-cell leukemia. Oncogene. 2007;26(8):1245-55.
26. Yamada Y, Ohmoto Y, Hata T, Yamamura M, Murata K, Tsukasaki K, et al. Features of the cytokines secreted by adult T cell leukemia (ATL) cells. Leuk Lymphoma. 1996;21(5-6):443-7.
27. Choi YL, Makishima H, Ohashi J, Yamashita Y, Ohki R, Koinuma K, et al. DNA microarray analysis of natural killer cell-type lymphoproliferative disease of granular lymphocytes with purified CD3(-) CD56(+) fractions. Leukemia. 2004;18(3): 556-65.
28. Hasegawa H, Yamada Y, Komiyama K, Hayashi M, Ishibashi M, Sunazuka T, et al. A novel natural compound, a cycloanthranilylproline derivative (Fuligocandin B), sensitizes leukemia cells to apoptosis induced by tumor necrosis factor related apoptosis-inducing ligand (TRAIL) through 15-deoxy-Delta 12, 14 prostaglandin J2 production. Blood. 2007;110(5):1664-74.
29. Chou TC, Talalay P. Quantitative analysis of dose-effect relationships: the combined effects of multiple drugs or enzyme inhibitors. Adv Enzyme Regul. 1984;22:27-55.
30. Yasunaga J, Taniguchi Y, Nosaka K, Yoshida M, Satou Y, Sakai T, et al. Identification of aberrantly methylated genes in association with adult T-cell leukemia. Cancer Res. 2004;64(17):6002-9.
31. Jacobs JJ, Kieboom K, Marino S, DePinho RA, van Lohuizen M. The oncogene and Polycomb-group gene bmi-1 regulates cell proliferation and senescence through the ink4a locus. Nature. 1999;397(6715):164-8.
32. Scott CL, Gil J, Hernando E, Teruya-Feldstein J, Narita M, Martinez D, et al. Role of the chromobox protein CBX7 in lymphomagenesis. Proc Natl Acad Sci USA. 2007;104(13):5389-94.
33. Cha TL, Zhou BP, Xia W, Wu Y, Yang CC, Chen CT, et al. Akt-mediated phosphorylation of EZH2 suppresses methylation of Lysine 27 in histone H3. Science. 2005;310(5746):306-10.
34. Varambally S, Cao Q, Mani RS, Shankar S, Wang X, Ateeq B, et al. Genomic loss of microRNA-101 leads to overexpression of histone methyltransferase EZH2 in cancer. Science. 2008;322(5908):1695-6.
35. Sander S, Bullinger L, Klapproth K, Fiedler K, Kestler HA, Barth TF, et al. MYC stimulates EZH2 expression by repression of its negative regulator miR-26a. Blood. 2008; 112(10):4202-12.
36. Godlewski J, Nowicki MO, Bronisz A, Williams S, Otsuki A, Nuovo G, et al. Targeting of the Bmi-1 oncogene/stem cell renewal factor by microRNA-128 inhibits glioma proliferation and self-renewal. Cancer Res. 2008;68(22):9125-30.
37. Cao R, Wang L, Wang H, Xia L, Erdjument-Bromage H, Tempst P, et al. Role of histone H3 lysine 27 methylation in Polycomb-group silencing. Science. 2002;298(5595): 1039-43.
38. Czermin B, Melfi R, McCabe D, Seitz V, Imhof A, Pirrotta V. Drosophila enhancer of Zeste/ESC complexes have a histone H3 methyltransferase activity that marks chromosomal Polycomb sites. Cell. 2002;111(2): 185-96.
39. Cao R, Zhang YI. SUZ12 is required for both the histone methyltransferase activity and the silencing function of the EED-EZH2 complex. Mol Cell. 2004;15(1):57-67.
40. Yu J, Yu J, Rhodes DR, Tomlins SA, Cao X, Chen G, et al. A polycomb repression signature in metastatic prostate cancer predicts cancer outcome. Cancer Res. 2007; 67(22):10657-63.
41. Bracken AP, Pasini D, Capra M, Prosperini E, Colli E, Helin K. EZH2 is down stream of the pRB-E2F pathway, essential for proliferation and amplified in cancer. EMBO J. 2003;22(20):5323-35.
42. Varambally S, Dhanasekaran SM, Zhou M, Barrette TR, Kumar-Sinha C, Sanda MG, et al. The polycomb group protein EZH2 is involved in progression of prostate cancer. Nature. 2002;419(6907):624-9.
43. Schlesinger Y, Straussman R, Keshet I, Farkash S, Hecht M, Zimmerman J, et al. Polycomb-mediated methylation of Lys27 of histone H3 pre-marks genes for de novo methylation in cancer. Nat Genet. 2007;39 (2):232-6.
44. Wei Y, Xia W, Zhang Z, Liu J, Wang H, Adsay NV, et al. Loss of trimethylation at lysine 27 of histone H3 is a predictor of poor outcome in breast, ovarian, and pancreatic cancers. Mol Carcinog. 2008;47 (9):701-6.
45. Sun F, Chan E, Wu Z, Yang X, Marquez VE, Yu Q. Combinatorial pharmacologic approaches target EZH2-mediated gene repression in breast cancer cells. Mol Cancer Ther. 2009;8(12):3191-202.
46. Cao P, Deng Z, Wan M, Huang W, Cramer SD, Xu J, et al. MicroRNA-101 negatively regulates Ezh2 and its expression is modulated by androgen receptor and HIF-1alpha/HIF-1beta. Mol Cancer. 2010;9: 108.
47. Bracken AP, Kleine-Kohlbrecher D, Dietrich N, Pasini D, Gargiulo G, Beekman C, et al. The polycomb group proteins bind throughout the INK4A-ARF locus and are disassociated in senescent cells. Genes Dev. 2007;21(5):525-30.
48. Morin RD, Johnson NA, Severson TM, Mungall AJ, An J, Goya R, et al. Somatic mutations altering EZH2 (Tyr641) in follicular and diffuse large B-cell lymphomas of germinal-center origin. Nat Genet. 2010; 42(2):181-5.
49. Yamada Y, Tomonaga M, Fukuda H, Hanada S, Utsunomiya A, Tara M, et al. A new G-CSF-supported combination chemotherapy, LSG15, for adult T-cell leukaemia-lymphoma: Japan Clinical Oncology Group Study 9303. Br J Haematol. 2001;113(2):375-82.
50. Ellis L, Pan Y, Smyth GK, George DJ, McCormack C, Williams-Truax R, et al. Histone deacetylase inhibitor panobinostat induces clinical responses with associated alterations in gene expression profiles in cutaneous T-cell lymphoma. Clin Cancer Res. 2008;14(14):4500-10.
51. Fiskus W, Wang Y, Sreekumar A, Buckley KM, Shi H, Jillella A, et al. Combined epigenetic therapy with the histone methyltransferase EZH2 inhibitor 3-deazaneplanocin A and the histone deacetylase inhibitor panobinostat against human AML cells. Blood. 2009;114(13):2733-43.

Open

Oncogene (2011) 1–12

www.nature.com/onc

ORIGINAL ARTICLE

TGF-β drives epithelial-mesenchymal transition through δEF1-mediated downregulation of ESRP

K Horiguchi[1], K Sakamoto[2], D Koinuma[1], K Semba[3], A Inoue[4], S Inoue[4], H Fujii[4], A Yamaguchi[2], K Miyazawa[5], K Miyazono[1] and M Saitoh[1,5]

[1]Department of Molecular Pathology, Graduate School of Medicine, University of Tokyo, Tokyo, Japan; [2]Section of Oral Pathology, Graduate School of Medical and Dental Sciences, Tokyo Medical and Dental University, Tokyo, Japan; [3]Department of Life Science and Medical Bio-Science, Waseda University, Tokyo, Japan; [4]First Department of Surgery, Interdisciplinary Graduate School of Medicine and Engineering, University of Yamanashi, Yamanashi, Japan and [5]Department of Biochemistry, Interdisciplinary Graduate School of Medicine and Engineering, University of Yamanashi, Yamanashi, Japan

Epithelial-mesenchymal transition (EMT) is a crucial event in wound healing, tissue repair and cancer progression in adult tissues. We have recently shown that transforming growth factor (TGF)-β-induced EMT involves isoform switching of fibroblast growth factor receptors by alternative splicing. We performed a microarray-based analysis at single exon level to elucidate changes in splicing variants generated during TGF-β-induced EMT, and found that TGF-β induces broad alteration of splicing patterns by downregulating epithelial splicing regulatory proteins (ESRPs). This was achieved by TGF-β-mediated upregulation of δEF1 family proteins, δEF1 and SIP1. δEF1 and SIP1 each remarkably repressed ESRP2 transcription through binding to the ESRP2 promoter in NMuMG cells. Silencing of both δEF1 and SIP1, but not either alone, abolished the TGF-β-induced ESRP repression. The expression profiles of ESRPs were inversely related to those of δEF1 and SIP in human breast cancer cell lines and primary tumor specimens. Further, overexpression of ESRPs in TGF-β-treated cells resulted in restoration of the epithelial splicing profiles as well as attenuation of certain phenotypes of EMT. Therefore, δEF1 family proteins repress the expression of ESRPs to regulate alternative splicing during TGF-β-induced EMT and the progression of breast cancers.
Oncogene advance online publication, 31 October 2011; doi:10.1038/onc.2011.493

Keywords: alternative splicing; δEF1; EMT; TGF-β; ESRP; breast cancer

Introduction

Splicing is a post-transcriptional process involved in the maturation of mRNAs and contributes to proteomic diversity by increasing the number of distinct mRNAs generated from a single gene locus. Recent works suggest that more than 90% of human genes can produce different isoforms through alternative splicing (Pan *et al.*, 2008; Wang *et al.*, 2008). This process is tightly regulated in a tissue- and cell-type-dependent fashion (Matlin *et al.*, 2005; Blencowe, 2006), and alterations in this process are often linked to various types of diseases including cancer (Wang and Cooper, 2007; Dutertre *et al.*, 2010). Aberrations of splicing machinery result from mutations in splicing sites or dysfunction of splicing regulatory factors (Licatalosi and Darnell, 2010).

One of the well-known genes that are regulated by tissue-specific alternative splicing is the fibroblast growth factor receptors (FGFRs). Functional FGFRs are encoded by four genes (FGFR1–FGFR4), and the receptors consist of three extracellular immunoglobulin domains (Ig-I, Ig-II and Ig-III), a single transmembrane domain and a cytoplasmic tyrosine kinase domain (Eswarakumar *et al.*, 2005). FGFRs have several isoforms, as exon skipping removes the Ig-I domain. In addition, alternative splicing in the second half of the Ig-III domain in FGFR1-FGFR3 produces the IIIb (FGFR1IIIb-FGFR3IIIb) and IIIc (FGFR1IIIc-FGFR3IIIc) isoforms that have distinct fibroblast growth factor (FGF)-binding specificities and are predominantly expressed in epithelial and mesenchymal cells, respectively. FGF-2 (basic FGF) and FGF-4 bind preferentially to the IIIc isoforms, whereas FGF-7 (keratinocyte growth factor) and FGF-10 bind exclusively to the IIIb isoforms (Coumoul and Deng, 2003; Chaffer *et al.*, 2007). Recently, epithelial splicing regulatory proteins (ESRPs) 1 and 2 were identified as coordinators of the epithelial cell-type-specific splicing program. ESRPs activate the splicing of exon IIIb and silence the splicing of exon IIIc of FGFR2, leading to the expression of proteins with the epithelial patterns of alternative splicing (Warzecha *et al.*, 2009a, b).

Epithelial-mesenchymal transition (EMT) is the differentiation switch directing polarized epithelial cells to trans-differentiate into mesenchymal cells (Thiery *et al.*, 2009). During the process of embryonic development, wound healing and reorganization in adult tissues, epithelial cells have been shown to lose their epithelial polarity and acquire mesenchymal phenotype. Further,

Correspondence: Professor K Miyazono or Dr M Saitoh, Department of Molecular Pathology, Graduate School of Medicine, University of Tokyo, 7-3-1 Hongo, Bunkyo-ku, Tokyo 113 0033, Japan.
E-mail: miyazono@m.u-tokyo.ac.jp or msaitoh-ind@umin.ac.jp
Received 6 April 2011; revised 25 July 2011; accepted 15 September 2011

EMT is involved in the process of invasion of tumor cells which also includes the loss of cell–cell interaction (Kalluri and Weinberg, 2009). Thus far, in nearly all cases, EMT appears to be regulated by extracellular matrix components and soluble growth factors or cytokines (Thiery and Sleeman, 2006). Among these factors, transforming growth factor-β (TGF-β) is considered as the key mediator of EMT during physiological processes. It is frequently and abundantly expressed in various tumors and also induces EMT in cancer cells during cancer progression. Recent studies revealed that TGF-β transcriptionally regulates expression of several transcription factors, including the zinc-finger factors Snail and Slug, the two-handed zinc-finger factors of δEF1 family proteins δEF1 and SIP1, the helix-loop-helix factors Twist and E12/E47, and the high motility group protein family HMGA2, which are involved in the induction of EMT particularly through the transcriptional repression of E-cadherin (Moustakas and Heldin, 2007; Miyazono, 2009).

We have recently reported that TGF-β induces isoform switching of FGFRs from IIIb to IIIc by alternative splicing during EMT in NMuMG cells, which results in enhanced EMT with aggressive phenotypes through cooperative action of TGF-β and FGF-2 (Shirakihara *et al.*, 2011). In the present study, we found that TGF-β regulates alternative splicing of numerous genes during EMT. The expression of δEF1 family proteins, δEF1 and SIP1, is increased after TGF-β treatment and subsequently represses the expression of the alternative splicing factor ESRP. Overexpression of ESRP in TGF-β-treated cells inhibits the conversion of alternative splicing pattern of epithelial types into those of mesenchymal types, as well as downregulation of the expression of E-cadherin. Repression of ESRP by δEF1 family proteins is thus, a crucial process during EMT induced by TGF-β and in progression of breast cancers.

Results

Changes in splice variants during TGF-β-induced EMT

We have recently found that TGF-β primes isoform switching of FGFRs by alternative splicing during TGF-β-induced EMT, thereby changing the sensitivities of cells from FGF-7 to FGF-2 (Shirakihara *et al.*, 2011). Reverse transcriptase-polymerase chain reaction (RT–PCR) analysis of mouse mammary epithelial NMuMG cells revealed that, in addition to *FGFRs*, *CD44* splicing profile and the total level of CD44 mRNA were changed after treatment with TGF-β (Figures 1a and b). There are multiple splice variants of the *Mena* gene (a member of Enabled (Ena)/vasodilator-stimulated phosphoprotein family of proteins) that are involved in cancer progression (Philippar *et al.*, 2008). We found that TGF-β also caused changes in splicing of the exon 11a of the *Mena* gene (Figure 1c). These findings suggest that alteration in splicing variants by TGF-β is not limited to FGFRs.

We next analyzed the expression of more than one million exons in NMuMG cells using mouse exon 1.0 ST array and adapted ARH method to rank the splicing predictions across the different genes (Figure 1d) (Rasche and Herwig, 2010). We found that the expression of 3601 genes was altered at the exon level, which was classified by GO parameters (Lee *et al.*, 2008), suggesting that TGF-β induces a broad alteration in splicing patterns and generates a number of splicing variants during EMT in NMuMG cells (Supplementary Figure S1 and Supplementary Table 1). As CD44, FGFRs, SLK (ste 20-like kinase) and CTNND1 (also known as δ-catenin or p120 catenin), of which splicing profiles have been reported to be regulated by ESRPs, were included in our exon-array data (Figure 1e and Supplementary Figure S2), we calculated ARH scores for the published exon-array data of ESRPs-silenced human prostate cancer PNT2 cells and compared the data with our exon-array data (Warzecha *et al.*, 2009b). We found that 227 genes and 75 genes in ESRP1/2-silenced cells overlapped with those of our data with $P<0.05$ and $P<0.01$, respectively (Supplementary Table 2). These findings suggest that TGF-β-induced changes in splice variants are partly mediated by ESRPs.

Repression of ESRPs by TGF-β

We next determined how TGF-β regulates the functions of splicing factors ESRP1 and ESRP2 during EMT. We found that TGF-β considerably downregulated the mRNA expression of ESRP2 in NMuMG cells, whereas the expression of ESRP1 mRNA could not be clearly detected (Figure 2a, left). We also examined the expression of ESRPs after TGF-β stimulation in other cells derived from mammary gland epithelial cells, including EpH4 cells expressing the viral H-Ras oncogene (EpRas cells) and breast cancer JygMC(A) cells (Ehata *et al.*, 2007). Treatment of EpRas cells with TGF-β repressed both ESRP1 and ESRP2 at the mRNA levels and ESRP1 at the protein level (Figures 2a, right and b). As JygMC(A) cells autonomously secrete TGF-β (Hoshino *et al.*, 2011), we treated the cells with TGF-β type I receptor (TβR-I) inhibitor, SB431542. The treatment increased the expression of ESRP1 and ESRP2 (Figure 2c). In addition, transfection of NMuMG cells with small interfering RNAs (siRNAs) against Smad2 and Smad3 attenuated the effects of TGF-β on the expression of ESRP2 (Figure 2d). Moreover, when *de novo* protein synthesis was inhibited by cycloheximide, which is an inhibitor of protein synthesis, downregulation of ESRP2 by TGF-β was attenuated (Figure 2e). PAI-1 and SIP1 have been reported as direct and indirect transcriptional targets of TGF-β/Smad pathway, respectively (Shirakihara *et al.*, 2007). Thus, these findings suggest that the suppression of ESRP2 by TGF-β involves *de novo* protein synthesis through the Smad pathway.

ESRP2 repression by δEF1 and SIP1 in TGF-β-induced EMT

We examined the expression profiles of δEF1, SIP1, E-cadherin and ESRP2 after TGF-β stimulation by quantitative RT–PCR. The levels of ESRP2 were

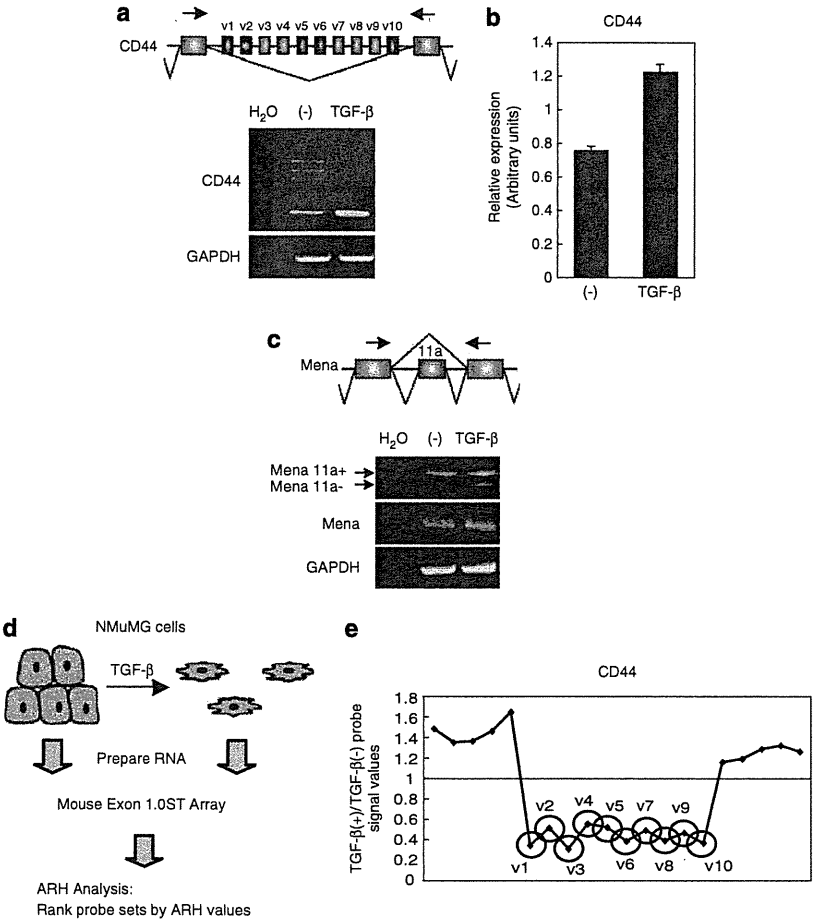

Figure 1 Changes in alternative splicing during TGF-β-induced EMT. (**a**) Changes in alternative splicing of CD44. Specific primers to detect v1-v10 variants of CD44 are shown as arrows (top panel). GAPDH was used as internal control. (**b**) The total level of CD44 mRNA was evaluated by quantitative RT–PCR analysis. (**c**) Specific primers to detect splicing variants of *Mena* are shown as arrows (top panel). GAPDH was used as internal control. (**d**) NMuMG cells treated with TGF-β for 24 h were prepared for Mouse Exon 1.0 ST Array. The ARH method was adapted to identify candidate genes at the exon level whose expressions changed during EMT. (**e**) The ratio of expression changes of each exon calculated by probe signal value in CD44 is shown. Red circles indicate the exons whose probe signals were altered by TGF-β treatment and reported to be spliced by ESRPs (Warzecha *et al*., 2009a).

gradually decreased until 24 h upon TGF-β stimulation, with the expression profile similar to that of E-cadherin and reciprocal to that of δEF1 and SIP1 (Figure 3a). To evaluate the mechanism of reciprocal regulation between δEF1/SIP1 and ESRP2 expression, we prepared the ESRP2 promoter region from NMuMG cells by a PCR-based strategy. The activity of ESRP2 promoter in NMuMG cells was remarkably repressed by constitutively active mutant of TβR-I (caTβR-I), δEF1 and SIP1. δEF1 overexpression had a stronger effect than SIP1 overexpression, probably because the protein levels of transfected SIP1 were much lower than those of δEF1 as determined by immunoblot analysis (Figure 3b and Supplementary Figure S3a). When we infected the cells with adenoviral vector encoding either δEF1 or SIP1, δEF1 or SIP1 each reduced the expression of endogenous ESRP2 mRNA with equivalent efficiencies (Figure 3c).

To determine whether δEF1 and SIP1 interact with the promoter regions of ESRP2, we performed chromatin immunoprecipitation (ChIP) assays in NMuMG cells after TGF-β treatment. The quality of commercially available anti-δEF1 antibody was appropriate for ChIP assays, whereas that of anti-SIP1 antibodies was not suitable for this assay. Thus, we overexpressed FLAG-tagged SIP1 in NMuMG cells and immunoprecipitated it with anti-FLAG antibody. In the absence of TGF-β, the level of δEF1 expression was very low and thus insufficient for ChIP (Figure 3d). After treatment with TGF-β, interactions of δEF1 with DNA fragments of the ESRP2 promoter in NMuMG and EpRas cells (Figure 3d, left and data not shown) and the ESRP1 promoter in EpRas cells (Figure 3d, right) were observed. Moreover, SIP1 also interacted with the ESRP2 and ESRP1 promoters, whereas neither δEF1 nor SIP1 associated with hemoglobin β gene (HBB) promoter that was used as a negative control (Figure 3d). In the competition assays of ChIP, overexpression of FLAG-SIP1 reduced the interaction of endogenous δEF1

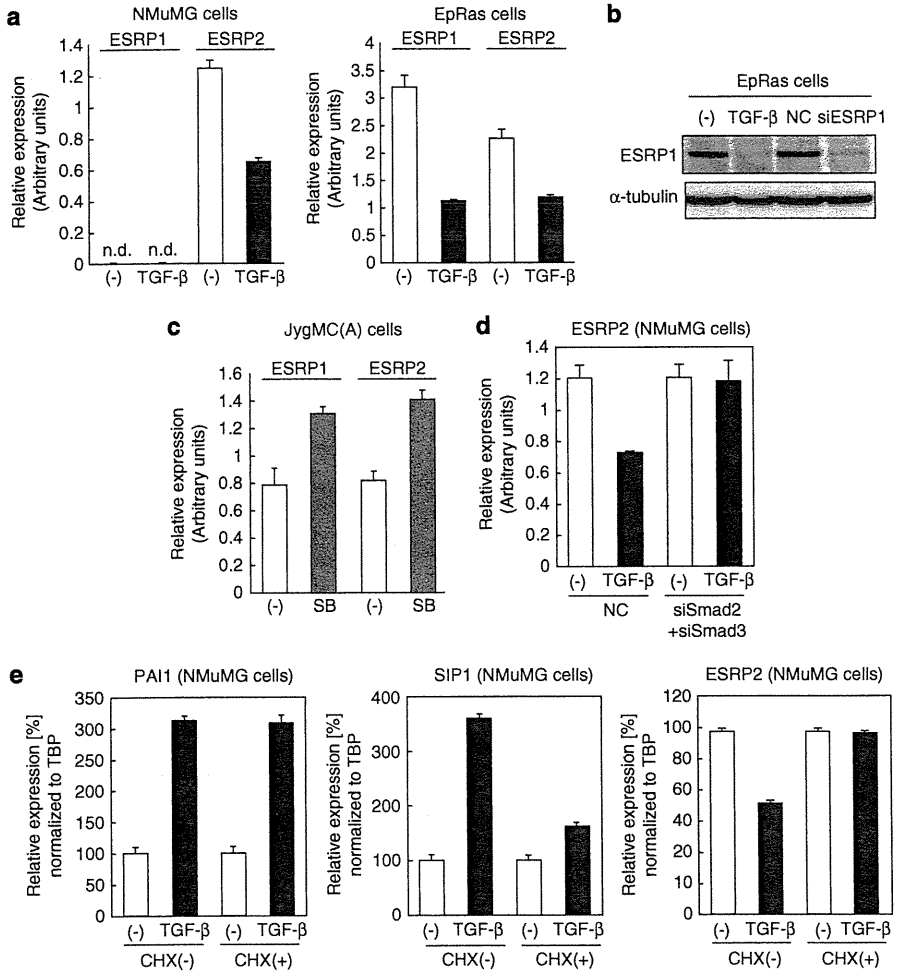

Figure 2 Requirement of *de novo* protein synthesis for downregulation of ESRP2 by TGF-β. (**a**) Effect of TGF-β on the expression of ESRPs in NMuMG cells (left) and EpRas cells (right) was examined by quantitative RT–PCR analysis. n.d., not detected. (**b**) After treatment of EpRas cells with TGF-β or transfection with ESRP1 siRNA, the levels of ESRP1 were evaluated by immunoblot analysis. α-tubulin was used as a loading control. (**c**) JygMC(A) cells were treated with 10 μM of TβR-I inhibitor (SB431542) for 48 h. The levels of ESRP1 and ESRP2 were evaluated by quantitative RT–PCR analysis. SB, SB431542. (**d**) NMuMG cells transfected with both Smad2 and Smad3 siRNAs were stimulated with 1 ng/ml TGF-β for 24 h, and then examined by quantitative RT–PCR analysis for the expression levels of ESRP2. NC, control siRNA. (**e**) NMuMG cells pretreated with 3 μM cycloheximide (CHX) for 1 h were stimulated with 1 ng/ml TGF-β for 24 h, and examined by quantitative RT–PCR analysis for PAI1 (left), SIP1 (center) and ESRP2 levels (right).

with the ESRP2 promoter (Supplementary Figure S3b), suggesting that δEF1 family proteins recognize the same binding regions of ESRP2 promoter. Overall, these findings indicate that δEF1 and SIP1 are preferentially recruited to the promoter region of ESRPs, and that they suppress the transcription of ESRPs in response to TGF-β treatment.

As double knockdown of δEF1 and SIP1 is necessary to block the E-cadherin repression by TGF-β (Shirakihara *et al.*, 2007), we next analyzed the TGF-β-mediated ESRP2 repression in NMuMG cells in which both δEF1 and SIP1 were silenced using their specific siRNAs (Figure 3e). TGF-β treatment induced the expression of δEF1 and SIP1 mRNAs by about three-fold after 48 h and repressed the expression of ESRP2. In the cells transfected with either δEF1 or SIP1 siRNA alone, TGF-β-mediated ESRP2 repression was only partially blocked; however, transfection with both δEF1 and SIP1 siRNAs completely abolished the TGF-β-mediated ESRP2 repression (Figure 3e). The δEF1/SIP1-mediated ESRP repression was also detected in EpRas cells (Supplementary Figure S3c). Therefore, similar to the repression of E-cadherin, the transcription of ESRPs is accumulatively regulated by the δEF1 family proteins during EMT by TGF-β.

Switching between FGFR isoforms by ESRPs during TGF-β-induced EMT

As we have previously reported (Shirakihara *et al.*, 2011), FGFR1 upregulated by TGF-β in NMuMG cells was the mesenchymal isoform, that is, FGFR1IIIc,

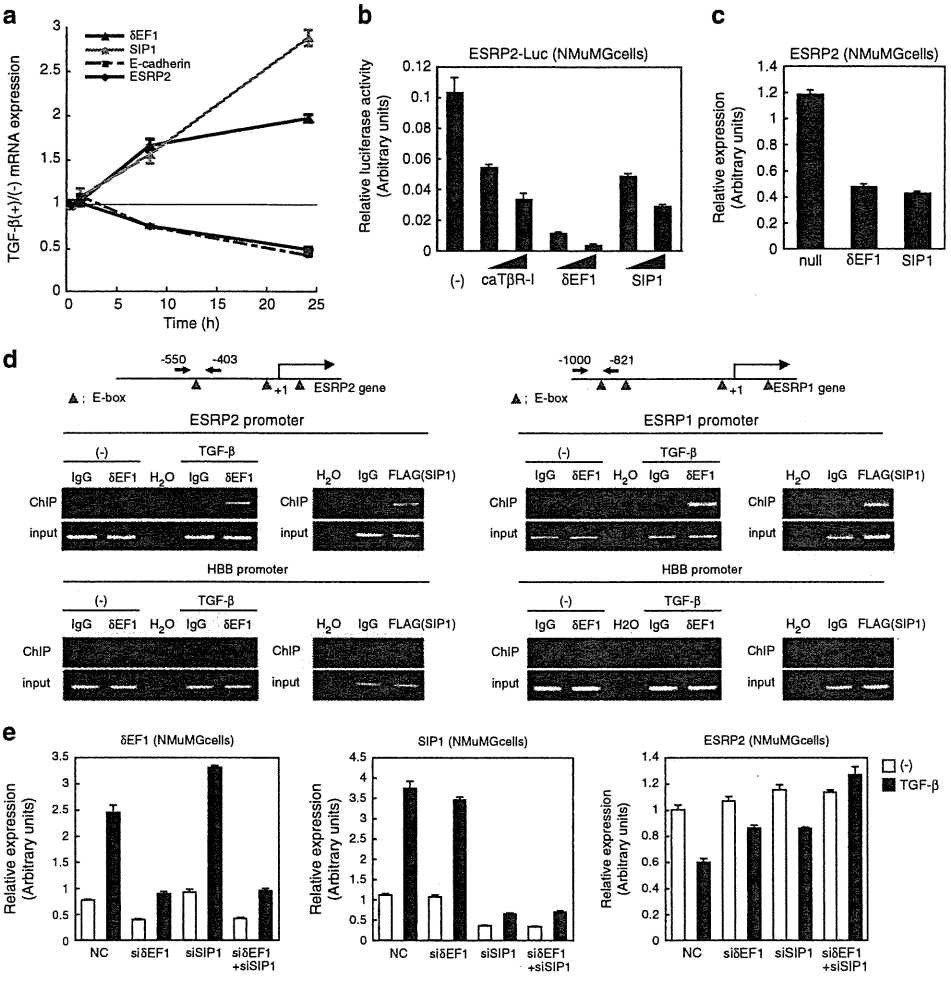

Figure 3 Regulation of ESRP2 expression by δEF1 and SIP1. (**a**) After treatment with 1 ng/ml of TGF-β, the kinetics of ESRP2, δEF1, SIP1 and E-cadherin expressions were examined in NMuMG cells by quantitative RT–PCR analysis. The ratio of the mRNA levels in TGF-β-treated cells as compared with that in non-treated cells is shown. (**b**) NMuMG cells were transfected with mouse ESRP2 promoter-reporter construct (ESRP2-Luc) in combination with various amounts of caTβR-I, δEF1 and SIP1 plasmids. At 48 h after transfection, cells were harvested and assayed for luciferase activities. (**c**) mRNA levels of ESRP2 in NMuMG cells infected with null, δEF1 or SIP1 adenoviruses were determined by quantitative RT–PCR. (**d**) ChIP analysis was performed using NMuMG and EpRas cells in the presence or absence of 1 ng/ml TGF-β. FLAG-SIP1 adenovirus was infected into NMuMG and EpRas cells 24 h before ChIP analysis. Endogenous δEF1 and FLAG-SIP1 were immunoprecipitated with anti-δEF1 antibody and with anti-FLAG antibody, respectively. Eluted DNAs from NMuMG cells and from EpRas cells were subjected to conventional PCR for ESRP2 promoter (left) and for ESRP1 promoter (right), respectively. HBB promoter was used as negative control. Primers used are shown as arrows. (**e**) NMuMG cells transfected with siRNA against δEF1, SIP1, or both (siδEF1 + siSIP1) were stimulated with 1 ng/ml TGF-β for 48 h and examined by quantitative RT–PCR analysis for δEF1 (left), SIP1 (center) and ESRP2 levels (right). NC, control siRNA.

whereas the FGFR2 downregulated by TGF-β was the epithelial isoform, that is, FGFR2IIIb (Figure 4a). Further, isoform switching of FGFR1 and FGFR2 was also observed in EpRas cells, in which both ESRP1 and ESRP2 were endogenously expressed (Figures 2a and 4b). Because TGF-β downregulated the total levels of FGFR2, the TGF-β-mediated induction of the IIIc isoform of FGFR2 was not clearly detected in both cells (Figures 4a and b). When ESRP2 was silenced by its specific siRNAs in NMuMG cells, ESRP2 siRNA changed the FGFR2IIIb isoform to FGFR2IIIc isoform without appearance of FGFR1IIIc in the absence of TGF-β (Figure 4c), suggesting that the TGF-β-mediated conversion of FGFR2IIIb into FGFR1IIIc requires ESRPs as well as other unidentified transcriptional factor(s). In addition, transfection with both ESRP1 and ESRP2 siRNAs in EpRas cells resulted in the expression of IIIc isoform of FGFR2 as well as that of FGFR1 (Figure 4d). Taken together, these findings suggest that TGF-β increases FGFR1 expression and decreases FGFR2 expression, leading to the conversion of the IIIb isoform into the IIIc isoform of FGFRs through alternative splicing by ESRPs.

We next performed gain-of-function experiments after achieving ectopic expression of FLAG-tagged ESRP2. After TGF-β treatment, the FGFR1IIIc isoform was